SUPPLEMENTARY INFORMATION

SUPPLEMENTARY EXPERIMENTAL PROCEDURES

Definition of EGFR-NCE and experimental determination of CME and NCE of the EGFR

Since the term 'NCE' encompasses many different internalization routes, it is important to give a precise definition of what we intend by the term "EGFR-NCE". We define this pathway operationally as: i) being clathrin-independent; ii) being dynamin-dependent; iii) being sensitive to the cholesterol-interfering drug filipin; iv) being caveolin-1-independent (Sigismund et al, 2008; Sigismund et al, 2005). In this paper, we also show that EGFR-NCE is absolutely dependent on the kinase activity of the EGFR.

Experimentally, NCE and CME of the EGFR were distinguished through clathrin-KD, which selectively blocks CME, or treatment with the cholesterol-blocking drug filipin, which selectively blocks EGFR-NCE (Sigismund et al, 2008). Typically, we measured the kinetics of ^{125}I-EGF internalization under four different conditions: i) WT cells (control si-RNA or mock-treated, as appropriate), ii) clathrin-KD cells, iii) filipin-treated cells, iv) clathrin-KD/filipin treatment. In some cases, an additional control, consisting of dynamin 2-KD cells was also included. An example of the typical kinetics is that depicted in Supplementary Figure 8A, B. From the kinetics, we calculated the Ke (either in the presence of low or high EGF doses).

We note that for high EGF doses, the kinetic parameter might not measure the actual endocytic rate constant, since at this dose bound counts might not remain constant over time. For this reason, we have used – throughout the paper – the more

appropriate term “observed Ke” (Ke obs, see also (Wiley & Cunningham, 1982), when describing the kinetics parameter at high EGF doses. We note, however, that in our experimental settings (i.e. in HeLa Milan cells and in NR6 cells transfected with EGFR), we observed only minor differences in the bound counts, in the time frames of our experiments (see Supplementary Figure 8A-B). This observation has two-fold consequences: i) also under conditions of high EGF, the Ke obs can be simply extrapolated by the first order internalization kinetics (Supplementary Figure 8A,B); ii) it is possible to compare directly the kinetics parameters obtained under low and high EGF.

We also note that in some of the cell lines shown in Table 1 (i.e. those displaying lower levels of surface EGFR, namely HCT116, BT549, MDA-MB-231, HeLa Oslo and HeLa Milan EGFR KD) we observed changes in bound counts within time at high EGF. Therefore, in these specific cases, we estimated the internalization coefficient Ke obs using the trapezoidal rule [see (Lund et al, 1990; Opresko & Wiley, 1987)].

For the data reported in Table 1, the presence of the NCE pathway was inferred from the comparison of the Ke values measured at low vs. high EGF doses, in the various conditions. In all cases, for low EGF doses, treatment with filipin did not change the Ke, with respect to the WT, while clathrin-KD reduced the Ke to values indistinguishable from those obtained under conditions of clathrin-KD/filipin or dynamin 2-KD. This confirmed that, at low dose EGF, the EGFR-NCE pathway is not operational, in all tested lines. At high dose EGF, we observed two different situations (based on the Ke values): A) “No NCE”, defined as control-WT = filipin > clathrin-KD = dynamin 2-KD (or clathrin-KD/filipin) (for MCF10A, HCT116, BT549, HeLa Oslo); “Yes NCE”, defined as control-WT > (either clathrin-KD or filipin) > (either

clathrin-KD/filipin or dynamin 2-KD) (for HeLa Milan, NR6-EGFR-WT, A431, MDAMB-231, BT20).

In Figure 9C,E and Supplementary Figure 12, we display the relative magnitude of CME and NCE in HeLa cells or in NR6 cells stably expressing EGFR add-back mutants, as a function of increasing EGF concentrations. In this case, measurements of ^{125}I-EGF internalization were performed at a single time point: 4 min for HeLa cells and 8 min for NR6 cells. These time points were chosen because they are in the linear phase of the internalization kinetics (see Supplementary Figure 8A,B) and are therefore representative of the Ke. We note that, at both high and low EGF concentrations, ~20-25% of the internalization events were insensitive to the combined clathrin-KD/filipin treatment or to the dynamin 2-KD, both in HeLa and NR6 cells (see for instance Table 1, Supplementary Figure 8A,B and Figure 3B). This might be due to the existence of an internalization pathway that is insensitive to these two conditions, or to an incomplete effect of the KD or drug treatment. We refer to this component operationally as "background endocytosis" (BE); in all calculations, this background (that was experimentally measured in each experiment) was subtracted, to obtain parameters unequivocally ascribable to CME and NCE (see also Supplementary Figure 8C,D for additional controls). After this normalization, the magnitude of CME was defined by two approaches: i) residual internalization under conditions of filipin treatment or ii) total internalization minus residual internalization under clathrin-KD. Both methods yielded comparable results.

Titanium sphere enrichment of phosphopeptides for MS analysis

Phosphopeptides were enriched using titanium sphere-chromatography (TiO2) columns, as previously described (Olsen et al, 2006), with minor modifications.

Acidified peptides (titrated below pH 2) were incubated with approximately 5 µL titanium sphere material (GL Sciences, Japan) in 0.5 g/L 2,5-dihydrobenzoic acid (DHB)/ 80% ACN / 0.1% TFA, for 30 min, under rotation. Beads were washed once with 100 µL 40% ACN/ 0.1% TFA and twice with 80% ACN/ 0.1% TFA and transferred to in-house produced C18-Stage Tips, mounted on 200 µL pipette-tips. The columns were washed one additional time with 80% ACN/ 0.1% TFA. Phosphopeptides were eluted from the TiO2-C8-Stage Tips into a 96-well plate with 40% ACN in 15 % ammonia-water solution (pH ~11) and dried to 2 µL in a vacuum concentrator (Eppendorf). Dried phosphopeptides were acidified with 0.1% TFA and directly subjected to LC-MS/MS analysis.

Mass Spectrometry Analysis (LC-MS/MS)

Peptides mixtures were analyzed by online nanoflow liquid chromatography tandem mass spectrometry (nanoLC-MS/MS), as described previously (Olsen et al, 2006). Briefly, all nanoLC-MS/MS-experiments were performed using an Agilent 1100 Series nanoflow LC system (Agilent Technologies), coupled to a 7-Tesla LTQ-FT-ICR-Ultra mass spectrometer (ThermoFisher Scientific, Bremen, Germany). The peptides were auto-sampled directly onto the 15 cm long 75 µm-inner diameter (i.d.) analytical column packed with reverse-phase C18 (ReproSil, Pur C18AQ 3 µm, Dr. Maisch, Germany) at a flow rate of 500 nl/min. The flow rate was reduced to 250 nl/min after loading, Solvent A was 0.1% FA and 5% ACN in ddH2O and solvent B was 95% ACN with 0.1% FA and the peptides were separated with a gradient of 2-40% solvent B over 100 min and 40-60% solvent B over 20 min. The effluent from the column was directly electro-sprayed into the mass spectrometer. The instrument, run under Xcalibur 2.0, was operated in the data-dependent mode to switch

automatically between full scan MS and MS/MS acquisition. Survey full scan MS spectra (from m/z 300 - 2000) were acquired in the ICR with resolution R=100,000 at m/z 400 (after accumulation to a 'target value' of 1,000,000). The five most intense multiply-charged ions ($z \geq 2$) were sequentially isolated and fragmented in the linear ion trap by collision- induced dissociation (CID), at a target value of 5,000 with a maximum ion time of 150 ms. Normalized CID collision energy was set to 35 % for MS/MS in LTQ and the ion selection threshold was set to 1000 counts. An activation q = 0.25 and activation time of 30 ms were used. Typical mass spectrometric conditions were: spray voltage, 2.5 kV; no sheath and auxiliary gas flow; heated capillary temperature, 190 °C.

MS analysis of phosphopeptides was carried out using instrument and method parameters as above, but with the following adjustments: tandem mass spectra were acquired with the multi-stage activation (MSA) option enabled for neutral losses of m/z 32.66, 48.99 and 97.97 (Schroeder et al, 2004); normalized CID collision energy was set to 40% for MSA in LTQ and ion selection threshold was set to 100 counts.

Assigning peptide sequences and quantitation using MaxQuant

MaxQuant, version 1.1.1.36, produced peak lists from the MS/MS spectra that are subjected to database search (Michalski et al, 2011). MS/MS spectra were recorded in "centroid" mode and the six most abundant peaks per 100 Da mass intervals were selected for search. Filtered MS/MS spectra were searched by Andromeda search engine (Cox et al, 2011) against the IPI human database version 3.68 (containing 87061 entries). IPI human version 3.68 database was combined with a list of 262 common contaminants, and concatenated with the reversed versions of all sequences (the so-called "Decoy database", (Kall et al, 2008)). Enzyme specificity was set to

trypsin, allowing cleavage N-terminal to Proline. Peptide identification was based on a search with mass deviation of the precursor ion of 7ppm and the fragment mass tolerance was set to 0.5 Da. The mass accuracy of the precursor ions was improved by the time-dependent recalibration (Cox et al, 2011). MaxQuant was employed to filter identifications at 1% false discovery rate (FDR) at three levels, namely: site, peptide, and protein. Up to two missed cleavages were allowed for trypsin digestion, Cysteine carbamidomethylation (Cys +57.021464 Da) was searched as fixed modification, whereas N-acetylation of protein (N-term, +42.010565 Da), oxidized Methionine (+15.994915 Da) were searched as variable modifications. To identify ubiquitination sites, searches were modified to allow GlyGly (+114.0429 Da) modification on Lysine. For phosphopeptide analysis, phosphorylation of Serine, Threonine and Tyrosine (Ser/Thr/Tyr, +79.966331 Da) were added as variable modifications. SILAC-based peptide- and protein-quantification were performed automatically by MaxQuant, taking into account all isotope patterns and all scans of the heavy and light forms of co-eluting peptide pairs (Cox et al, 2009), (see Supplementary Table 1, datasheets A and B). Finally, for each peptide the modification site was assigned and the confidence of the assignment was expressed by means of the "localization probability" parameter (equal to 1 in the four modified peptides reported in Supplementary Table 1, datasheet C) (Nagaraj et al, 2010; Olsen et al, 2005).

AG1478 treatment

Treatment was performed by pretreating cells with 150 nM or 250 nM AG1478 for 20 min at 37˚C, followed by performance of internalization assays in the contiunuos presence of the compound.

Size exclusion chromatography

Size exclusion chromatography was performed as described (Penengo et al, 2006), starting from a cellular lysate of HeLa cells prepared in JS buffer (50 mM Hepes pH 7.5, 50 mM NaCl, 1% glycerol, 1% Triton-X100, 1.5 mM MgCl, 25 mM EGTA), plus protease and phosphatase inhibitors (see Materials and Methods). Before chromatography, lysates were subjected to ultracentrifugation for 1 h at 120,000 g.

SUPPLEMENTARY FIGURE LEGENDS

Supplementary Figure 1. Additional data supporting the concept of the ubiquitination threshold. A. Quantitative assessment of the blots shown in Figure 1A, expressed as a percentage of the maximal tyrosine phosphorylation or ubiquitination (% of max, see Materials and Methods). **B**. Quantitative assessment of the blots shown in Figure 1B, expressed as a percentage of the maximal tyrosine phosphorylation (% of max). **C.** HeLa cells were stimulated with the indicated concentrations of EGF for 2 min. IP and IB were performed as indicated (Ub, ubiquitin P4D1 antibody). Note that there is no further increase in EGFR-pY (and Ub) between 100 and 300 ng/ml of EGF treatment, meaning that at 100 ng/ml the maximum level of receptor modification has been reached. For this reason, we performed all our dose-response curves up to a maximum of 100 ng/ml of EGF. Actual IBs are in the top panel, and a quantitation of the results is in the bottom panel **D.** To verify that the Ub signals observed by IB in anti-EGFR IP were due exclusively to EGFR ubiquitination and not to co-immunoprecipitating proteins, we repeated the experiment shown in Figure 1A of the main text by lysing cells in RIPA buffer containing 1% SDS (see Materials and Methods). Also under these stringent lysis conditions, the Ub threshold was readily detected and indistinguishable from that obtained under standard conditions of cell lysis. Left, HeLa cells were stimulated with EGF for 2 min at the indicated concentrations. Lysates were prepared in 1% SDS-containing lysis buffer (followed by dilution, after lysis, to a final 0.2% SDS concentration, see Materials and Methods) and subjected to IP and IB as shown. Right, quantitation of the blots shown as % of max. The red curve shows detection with the P4D1 Ab on lysates prepared with standard RIPA buffer (0.1% SDS, as in all

the IB experiments of the main text, unless otherwise specified**)** and was taken from the quantitative measurements shown in panel A, top. **E.** In this experiment, we characterized different anti-Ub antibodies for EGFR-Ub threshold recognition. This represents an important control to verify that the Ub threshold is not an artifact due to a specific anti-Ub antibody recognition pattern. Importantly, the same threshold behavior was observed with all antibodies. Left, HeLa cells were stimulated with EGF for 2 min at the indicated concentrations. Lysates were subjected to IP anti-EGFR and IB with two different anti-Ub antibodies (FK2, used in all ELISA experiments, and ZTA10). Right, quantitation of the blots shown as % of max. The red curve shows detection with the P4D1 Ab (which was used in all the IB experiments of the main text, unless otherwise specified**)** and was taken from the quantitative measurements shown in panel A, top. **F.** In most of the experiments shown, a polyclonal anti-EGFR antibody (generated in house) was used, which recognized the C-terminal tail (the last amino acids containing the Y1173 phosphorylation site). In order to exclude competition between phosphorylation at Y1173 site and antibody recognition, we repeated the experiment shown in Figure 1A of the main text using an antibody directed against the extracellular domain with comparable results. Left, HeLa cells were stimulated with EGF for 2 min at the indicated concentrations. Lysates were subjected to IP with antibodies either recognizing an EGFR intracellular epitope (aa 1172-1186, which was used in all the IB experiments of the main text, unless otherwise specified) or an extracellular one (Ab-1 from CALBIOCHEM). IB was as shown. Right, quantitation of the blots shown as % of max.

In all panels, error bars indicate standard deviation calculated on at least three independent experiments. R, Pearson correlation coefficient.

Supplementary Figure 2. Additional information on the ELISA assay. A, B. Scheme of the "forward" and "reverse" approaches. **A.** In the "forward" approach, microwell plates were coated with a polyclonal anti-EGFR antibody (intracellular domain), which captures the receptor from the lysate (1). Detection of Ub-EGFR, pY-EGFR or total EGFR was performed with primary monoclonal antibodies directed against Ub (FK2), or pY (4G10) or EGFR (m108, extracellular domain) (2), followed by Europium (Eu)-labeled secondary antibodies (3). **B.** In the reverse approach, microwell plates were coated with monoclonal antibodies directed against Ub (FK2), or pY (4G10) or EGFR (m108) that capture Ub-EGFR (1), pY-EGFR (2) or total EGFR (3), respectively. Detection was performed with a polyclonal anti-EGFR antibody (intracellular domain) followed by a Eu-labeled secondary antibody. **C.** Comparison of EGFR ubiquitination (top) or phosphorylation (bottom) curves obtained by IB (from Supplementary Figure 1A, top) and ELISA (from Figure 1C).

In all panels, error bars indicate standard deviation calculated on at least three independent experiments. P-values were calculated using two-way ANOVA analysis. When comparing curves that showed significant differences, we show the relative p-values; when comparing curves that did not show significant differences, we display R, the Pearson correlation coefficient. In panel C, the asterisk indicates the only point that significantly differed in the two curves ($p = 0.01$). This, however, does not affect the interpretation of the results, since both methods detect a threshold positioned within the same range of EGF doses. Moreover, ELISA curve exhibited an even sharper threshold effect than the IB curve.

Supplementary Figure 3. Additional details on SILAC-MS approach. A. Scheme of the experiment for sample preparation, MS analysis and data processing. Tryptic

peptides from EGFR in-gel digestion were so divided: 70% of the sample was loaded on C18-Stage Tips for standard MS analysis; 30% was subjected to phospho-enrichment on TiO2 beads and then MS analyzed. Quantification of both proteins and phosphopeptides was carried out with MaxQuant. **B, C.** Representative MS signals in survey scan corresponding to ubiquitin (UBC, panel B) and EGFR peptide (panel C) identified and quantified in each IP-SILAC experiment. Ions with m/z values of 894.4697, 898.4780 (panel B) and 995.5594, 1000.0620 (panel C) are identified as [M +2H]2+ SILAC pairs of UBC (11-27) TITLEVEPSDTIENVK and EGFR (81-98) TIQEVAGYVLIALNTVER, respectively. Visual inspection of UBC peptide pairs indicates increase of abundance upon EGF stimulation, whereas total amount of EGFR remains constant in the same conditions as measured with its peptide ratios, and close to value 1 (see also Figure 2C-D). **D.** SILAC MS quantitation of EGFR Y(1148). Ions with m/z values of 1158.5082, 1162.5150 are identified as [M+2H]2+ SILAC pairs of EGFR (1137-1155) GSHQISLDNPDpYQQDFFPK phosphopeptides. **E.** SILAC MS quantitation of EGFR Y(1173). Ions with m/z values of 645.7730, 650.7779 are identified as [M+2H]2+ SILAC pairs of EGFR (1065-1075) GSTAENAEpYLR phosphopeptides. **F.** SILAC MS quantitation of EGFR Y(1086). Ions with m/z values of 827.0735, 833.7447 are identified as [M+2H]2+ SILAC pairs of EGFR (1076-1097) RPAGSVQNPVpYHNQPLNPAPSR phosphopeptides. **G.** SILAC MS quantitation of EGFR/Ub-K(692). Ions with m/z values of 777.4410, 785.4554 are identified as [M+2H]2+ SILAC pairs of EGFR (691-704) IK(gg)VLGSGAFGTVYK ubiquitinated peptides. **H-K.** Annotation of Tyrosine (Y) phosphorylation and Lysine (K) sites on EGFR. **H.** Annotated MS/MS CID (collision induced dissociation) spectrum of EGFR peptide GSHQISLDNPDpYQQDFFPK. The fragmentation leads to 74% of amino acid

coverage, allowing the identification of tyrosine 1148 phosphorylated on EGFR. **I.** Annotated MS/MS CID spectrum of the peptide GSTAENAEpYLR. The fragmentation leads to 82% amino acid coverage allowing the identification of tyrosine 1173 phosphorylated on EGFR. **J.** Annotated MS/MS CID spectrum of RPAGSVQNPVpYHNQPLNPAPSR peptide. The fragmentation leads to 82% amino acid coverage, which allows identification of Tyrosine 1086 phosphorylation. **K.** Annotated MS/MS CID spectrum of IK(gl)VLGSGAFGTVYK peptide. The fragmentation leads to 86% amino acid coverage, which allows identification of ubiquitination at Lysine 692.

Supplementary Figure 4. Analysis of Cbl and Grb2 elution profiles by size exclusion chromatography. This experiment allowed us to better understand the behavior of Grb2 in the co-IP experiments with EGFR, upon increasing EGF concentrations (Figure 4D of the main text). If the Cbl:Grb2 complex had existed at a high stoichiometry, Grb2 might have shown the same behavior of Cbl (i.e. threshold binding to the EGFR with increasing EGF concentrations), while instead it displayed gradual increments in binding to the receptor. However, as shown in this Supplementary Figure by size exclusion chromatography, in living cells most Grb2 is free, while Cbl is predominantly present in complexes that also contain Grb2. Thus, *in vivo*, the shape of the Grb2:EGFR association curve would be determined essentially by free Grb2, thereby displaying a typical hyperbolic association curve (which translates in a quasi-linear shape when a log-scale is used, see Figure 4D). Furthermore, the *in vivo* association of Grb2 with the EGFR add-back mutants (Figure 7D of the main text) corroborated the idea that a small fraction of Grb2 is associated to Cbl (thus explaining its binding to the 1045+ mutant), while the majority of it

exists in a free form (that binds to the 1068/86+ mutant – which does not bind to Cbl – as efficiently as it does to EGFR-WT or to the 1045/1068/1086+ mutant).

HeLa cell lysates were subjected to size exclusion chromatography. Equal amounts of the fractions were loaded on SDS-PAGE and IB as indicated. I, input (50 μg). In the Grb2 panels: s.e. and l.e., represent short and long exposure, respectively.

Supplementary Figure 5. Phosphorylation of Cbl by EGFR WT or add-back mutants. The association *in vivo* between Cbl and EGFR displayed a threshold behavior as a function of EGF dose (Figure 4D). However, Cbl-pY increased gradually upon EGF dose escalation (Figure 5B). To explain this apparent discrepancy, we reasoned that even a weak (and transient) interaction – such as that determined by the presence of a single Cbl-binding phosphosite – might be sufficient for the EGFR kinase to phosphorylate Cbl. If this were the case, individual Cbl-binding phosphosites should drive Cbl phosphorylation independently of each other and not show any synergistic effect. To test this hypothesis we exploited the EGFR add-back mutants displaying a strong (EGFR WT or 1045/68/86+) or weak (1045+ or 1068/86+) association with Cbl (Figure 7D and 8A). As shown in this Figure, the Y1045+ or Y1068/86+ add-back mutants displayed efficient phosphorylation of Cbl, which reached a maximum level of around one half of that obtained with the 1045/68/86+. The effect of the re-engineering of the double Cbl-binding surfaces (in the 1045/68/86+ mutant) was additive, and not synergistic, with respect to individual surfaces, in sharp contrast to what was observed for the association between Cbl and the various add-back mutants (see Figure 7D). This is compatible with the original hypothesis that while Cbl requires a stable interaction in order to act as an E3 ligase

towards the EGFR, a weak/transient binding is sufficient for Cbl to serve as a phosphorylation substrate for the EGFR kinase.

Top, NR6 cells, stably transfected with the indicated EGFR constructs, were stimulated with EGF for 2 min at 100 ng/ml, followed by IP and IB as shown. Bottom, quantitation of the blots.

Supplementary Figure 6. Characterization of EGFR Y-to-F mutants. As a preliminary approach to the experimental challenge of the cooperativity model (Figure 5A), we employed a series of EGFR mutants. Indeed, a prediction of the cooperativity model is that elimination of one of the two interaction surfaces on the EGFR should severely impair the recruitment of Cbl and the ensuing EGFR ubiquitination. Thus, we engineered EGFR mutants (Y-to-F) in which the relevant Tyr residues were mutagenized to Phe, alone or in combination (panel A). The resulting mutants Y1045F, Y1068/1086F, and Y1045/1068/1086F (TripleF) were transfected in NR6 cells and exhibited similar levels of surface expression (panel B). As a negative control, we used a kinase-inactive EGFR mutant (K721A, panels A, B). The Y-to-F mutants were analyzed for their tyrosine phosphorylation using specific anti-phosphoEGFR Abs (panel C) or binding to GST-Grb2 or GST-Cbl (panel D, top and bottom, respectively), and behaved as expected.

We then tested the EGF-induced ubiquitination of the Y-to-F mutants. The mutagenesis of either Y1045 or the doublet Y1068/1086 severely diminished EGFR ubiquitination, while the TripleF mutant displayed marginally detectable ubiquitination (panel E, top). By densitometric analysis of several independent experiments and blot exposures, we established that the TripleF mutant is ubiquitinated at < 3% of the levels detected in EGFR-WT. Of note, the sum of the

residual EGFR ubiquitination in the Y1045F (~ 10%) and Y1068/1086F (~ 30%) mutants did not add up to the level displayed by EGFR-WT (panel E, bottom). This finding supports the cooperativity model, which predicts a synergistic, rather than additive, interaction between these two phosphosites. In addition, there seems to be a hierarchy between the two sites, with Y1045 being a stronger determinant than Y1068/1086 in driving EGFR ubiquitination.

The dramatically reduced ubiquitination of the TripleF mutant allowed us to test the hypothesis that EGFR ubiquitination is the predominant signal for committing the receptor to NCE, while being dispensable for EGFR-CME. This hypothesis was previously put forward based on data showing that the Y1045F mutant, whose ubiquitination is impaired, is internalized exclusively through CME (Jiang & Sorkin, 2003; Sigismund et al, 2008; Sigismund et al, 2005). However, it has been argued that residual ubiquitination displayed by the Y1045F mutant might in principle be sufficient to couple the EGFR with CME (Grovdal et al, 2004; Huang et al, 2006; Kazazic et al, 2009; Madshus & Stang, 2009). Indeed, from our measurements, the Y1045F mutant displays, once ectopically expressed in NR6 cells, around 10% of the EGFR WT ubiquitination (panel E). The TripleF mutant (Y1045/68/86F), conversely, displays < 3% ubiquitination (panel E). Thus, we tested internalization of EGFR WT and the TripleF mutant under different conditions (panel F). EGFR WT displayed the previously characterized pattern of internalization (Sigismund et al, 2008; Sigismund et al, 2005), being completely sensitive to blockade of CME (clathrin-KD) at low EGF concentrations, and partially sensitive to the inhibition of either CME or NCE (filipin treatment) at high concentrations. The TripleF mutant, displayed overall good internalization (~ 60% of EGFR WT at both low and high concentrations). However, the mutant was internalized almost exclusively through CME. Thus, the analysis of

the TripleF mutant supports the notion that EGFR ubiquitination is essential for NCE, while it is dispensable for CME of the EGFR.

A. Scheme of the Y-to-F mutants used in this study. The intracellular domain, comprising the kinase domain and the C-terminal tail, of the EGFR is shown, with the positions of relevant residues. Mutagenized residues are indicated in red. **B**. NR6 cells stably expressing EGFR WT or the indicated mutants were analyzed by ^{125}I-EGF saturation binding and the number of surface receptors was measured. Data are expressed as surface EGFRs/cell. **C.** NR6 cells stably expressing EGFR WT or the indicated mutants were stimulated with EGF (100 ng/ml, 2 min). Lysates were subjected to IB as indicated. **D.** NR6 cells stably expressing the indicated mutants were stimulated with EGF (100 ng/ml, 2 min). Lysates were subjected to pull-down assays with either GST-Grb2 (top) or GST-Cbl (bottom). Detection was by Ponceau staining or IB with anti-EGFR. **E**. Top, NR6 cells stably expressing the indicated mutants were stimulated with EGF (100 ng/ml, 2 min). Lysates were subjected to IP and IB, as shown. Bottom, quantitative assessment of the blots shown in the upper panel. Results are expressed as arbitrary units (100 = max WT, see Materials and Methods). "Theor. Sum" is the theoretical sum of the signals obtained with the Y1045 and Y1068/1086 mutants. **F.** ^{125}I-EGF internalization of EGFR WT and the TripleF mutant. Results are expressed as internalization rate constants (Ke) and are the mean of triplicate points (s.e.m. < 8%).

Supplementary Figure 7. EGFR add-back mutants: autophosphorylation and phosphorylation of Cbl. The EGFR add-back mutants were analyzed for their ability to phosphorylate the residual Tyrosine residues, and they exhibited EGF dose-response curves comparable to EGFR-WT. Indeed, as shown in this Figure, the levels

of pY1045 and pY1068 were comparable in EGFR-WT, EGFR-1068/86+ (A), EGFR-Y1045+ (B) or EGFR-1045/68/86+ (C). This experiments shows that: i) the intrinsic kinase activity of the add-back mutants is comparable to EGFR-WT; ii) EGFR phosphorylation events, at least for the two analyzed phosphosites, do not depend on each other, i.e., do not take place according to a hierarchy of phosphorylations, in agreement with previously reported data (Olsen et al, 2006); iii) the phosphorylation of the two Cbl binding sites (Y1045 and Y1068) does not depend on the phosphorylation status of other Tyrosines.

A, B, C. NR6 cells, stably transfected with the indicated EGFR constructs, were stimulated with EGF at the indicated doses, followed by IP and IB as shown. Quantitation of the blots is shown in Figure 7 C of the main text.

Supplementary Figure 8. Additional controls of ^{125}I-EGF internalization kinetics in HeLa and NR6 cells. A. Internalization kinetics of HeLa cells using ^{125}I-EGF at low (1 ng/ml, top panel) or high (30 ng/ml, bottom panel; the bound counts are also shown for the high EGF condition) EGF concentrations. In both conditions, internalization is linear between 2 and 6 min, and endocytic rate constants (Ke and Ke obs, see Supplementary Experimental Procedure) were calculated from the slope of the trend-line. The 4 min time-point (in the linear phase) was chosen for the studies shown in Figure 9B-C of the main text. **B.** Internalization kinetics of NR6 cells expressing EGFR-WT using ^{125}I-EGF at low (1 ng/ml, top panel) or high (30 ng/ml, bottom panel; the bound counts are also shown for the high EGF condition) EGF concentrations. In both conditions, internalization is linear between 4 and 12 min, and endocytic rate constants (Ke and Ke obs, see Supplementary Experimental Procedure) were calculated from the slope of the trend-line. The 8 min time-point (in the linear

phase) was chosen for the studies with add-back mutants shown in Figure 9D-E of the main text and in and in Supplementary Figure 12. **C, D. EGFR kinase activity and EGFR internalization.** The rationale of this experiment was to understand whether EGFR-NCE and -BE (background endocytosis) are kinase-dependent. This was tested by inhibiting the EGFR kinase activity, in HeLa cells, with a specific inhibitor (AG1478, panel C) or exploiting an EGFR kinase-dead mutant (K721A) stably expressed in NR6 cells (panel D). At the tested doses (150 and 250 nM), AG1478 treatment inhibited EGFR autophosphorylation at major Tyr sites (C, top). AG1478 treatment reduced ^{125}I-EGF internalization by ~80% at both low and high EGF concentrations, an effect comparable to that obtained by dynamin 2 KD (C, bottom panels). Of particular interest are the effects of AG1478 on EGFR-NCE and EGFR-BE, from which it can be concluded that:

1) EGFR-NCE. Under conditions of high EGF, the residual internalization upon clathrin KD is the sum of NCE and BE. The magnitude of the BE component, under these conditions, is established by dynamin 2 KD. Treatment with AG1478, reduced EGF internalization to the levels observed in the presence of dynamin 2 KD. Furthermore, the combined clathrin KD/AG1478 treatment did not have additive effects with respect to AG1478 alone (a slight reduction was observed which however did not reach statistical significance, $P > 0.5$). This result corroborates the idea that EGFR-NCE depends on the kinase activity of the EGFR.

2) EGFR-BE. Both at low and EGF doses, BE is defined as the residual internalization upon dynamin 2 KD. The combined dynamin 2 KD/AG1478 treatment did not have additive effects with respect to individual treatments, at either dose of EGF (a slight reduction was observed which however did not reach statistical significance, $P > 0.5$). This result supports the concept that EGFR-BE does not

depend on the kinase activity of the EGFR and probably represent a constitutive form of receptor internalization.

In the AG1478 experiments, there was a small trend towards a further reduction in the internalization rates when the inhibitor was administered in conjunction with the KD of clathrin or of dynamin 2, vs. the KD alone. As already mentioned, this reduction never attained statistical significance and we attributed it to residual levels of CME and/or NCE due to incomplete KD of the proteins. Nevertheless, we thought that our general conclusions could benefit from further support by an independent approach. To this end, we exploited an EGFR kinase-dead mutant (K721A) stably expressed in NR6 cells (panel D). This mutant is not internalized through either CME or NCE (as shown in the Figure, it is insensitive to filipin or clathrin KD at both EGF doses), and it displays only background endocytosis (~25% of the levels of EGFR-WT), further re-enforcing the notion that EGFR-NCE depends on the kinase activity of the receptor while EGFR-BE does not.

C. Top, HeLa cells pre-treated, or not, for 20 min with 150 nM or 250 nM of AG1478 were stimulated or not for 2 min with 100 ng/ml EGF in the presence or absence of the inhibitor. Lysates were subjected to IB with the indicated antibodies. Note that the anti-EGFR IB was assembled with lanes from the same gel, to remove an irrelevant molecular weight marker lane. Bottom, ^{125}I-EGF internalization in HeLa cells subjected to clathrin KD or dynamin 2 KD and treated or not with AG1478 as indicated. Results are expressed as the internalization rate constant (Ke or Ke obs, see Supplementary Experimental Procedure) and are the mean of triplicate experiments.

D. ^{125}I-EGF internalization of EGFR WT and K721A mutant at 8 min upon low (1 ng/ml) or high (30 ng/ml) EGF concentration. Results are expressed as internalized/bound ^{125}I-EGF and are the mean of triplicate experiments.

Supplementary Figure 9. Efficacy of the KD procedures in the various cell lines displayed in Table 1. This series of blots shows the level of KD achieved for either clathrin heavy chain (Clath-KD) or dynamin 2 (Dyn-KD), in the indicated cell lines, in the experiments aimed at measuring the presence of EGFR-NCE (depicted in Table 1). Cells were subjected to clathrin-KD or dynamin 2-KD as described in Materials and Methods. The level of KD was analyzed by IB with the indicated Abs 48h after the second RNAi transfection. The silencing of clathrin and dynamin was efficient in all cell lines tested at comparable levels.

Supplementary Figure 10. Efficacy of Cbl KD in the experiments reported in Figure 9A. This Supplementary Figure shows the levels of silencing obtained in the cellular populations employed in the internalization experiments shown in Figure 9A of the main text. HeLa cells were subjected to Cbl KD, alone or in combination with clathrin KD or dynamin 2 KD as indicated (Control, HeLa cells transfected with control oligo). IB was as shown (Tub, tubulin; loading control).

Supplementary Figure 11. Effects of Grb2 KD on NCE. A prediction of our of model is that EGFR-NCE should be dependent on Grb2, similar to its dependence on Cbl. To verify this prediction we performed Grb2 silencing in HeLa cells and tested EGFR internalization. Both at low and EGF doses, Grb2 KD reduced internalization rates to those present in dynamin 2-KD cells. This is consistent with the idea that both CME [as also shown by others, (Huang et al, 2004)] and NCE are Grb2-dependent, while BE is not (as also further shown by the fact that there was no additive effect of the double Grb2/dynamin 2 KD). Note that under conditions of high EGF, the double

Grb2/clathrin KD inhibited internalization to a much greater extent than the clathrin KD alone, further showing that EGFR-NCE is Grb2-dependent.

Top, HeLa cells were subjected to Grb2KD, alone or in combination with clathrin KD or dynamin 2 KD (Control, HeLa cells transfected with control oligo). IB was as shown (Tub, tubulin; loading control). Bottom, ^{125}I-EGF internalization kinetics in control HeLa cells or upon KD of the indicated proteins at low (1 ng/ml) or high EGF dose (30 ng/ml). Results are expressed as internalization rate constants (Ke or Ke obs) and are the mean of triplicate experiments. As a control, Transferrin (Tf) internalization was also assessed, by ^{125}I-Tf. As previously reported, Tf internalization was Grb2-independent (Huang et al, 2004).

Supplementary Figure 12. Controls for EGFR-WT and EGFR mutants in NR6 cells. A. ^{125}I-EGF internalization of EGFR-WT and of the indicated mutants in NR6 cells, under conditions of clathrin-KD or filipin treatment. Internalization was measured at 8 min in the presence of low EGF (L, 1 ng/ml) or high EGF (H, 30 ng/ml). Results are expressed as internalized/bound ^{125}I-EGF and are the mean of triplicate points (s.e.m. < 8%). See Supplementary Experimental Procedures for additional details. While this experiment represents an initial characterization of the internalization properties of the add-back mutants, it portrays a number of aspects not included in the more extended analyses presented in Figure 9D-E of the main text. In particular: i) the 9Y- and 1068/1086+ mutants displayed negligible internalization, at both low and high EGF concentrations, which was barely above the background endocytosis of the kinase-inactive K721A mutant; ii) the 1045+ mutant showed clearly detectable internalization at both EGF concentrations albeit reduced with respect to EGFR-WT. At low EGF, internalization was exclusively through CME;

while at high EGF, internalization was through both CME and NCE. While the NCE internalization of the 1045+ mutant is not surprising (NCE depends on EGFR ubiquitination and the 1045+ mutant is ubiquitinated, although with reduced efficiency compared with EGFR-WT), the CME-mediated internalization was less expected and is discussed in the Discussion section of the main text. **B.** Dose response curves of ^{125}I-EGF internalization and EGFR ubiquitination (measured by ELISA, forward approach) in NR6 cells expressing 1045+ add-back mutant. CME and NCE are shown, determined as explained in Supplementary Experimental Procedures. Only the profiles of the curves are shown. The actual data from which the curves were calculated and drawn are in Figure 8C (for Ub) and Figure 9E of the main text.

SUPPLEMENTARY TABLE

Supplementary Table 1 is provided as a separate .xls file

Supplementary Table 1. Extracted data from MaxQuant analysis for UBC and EGFR peptides (assignment and quantitation). A. Summary of ubiquitin (UBC) and EGFR proteins identification and MaxQuant- based SILAC quantitation. **B.** List of peptides assigned to UBC and EGFR and analytical and statistical parameters for peptide ID. **C.** Attribution of modification sites and MaxQuant quantitation of EGFR phosphotyrosines 1068, 1148, 1173 and ubiquitination at Lysine 692 (Cox et al, 2009).

REFERENCES TO SUPPLEMENTARY INFORMATION

Cox J, Matic I, Hilger M, Nagaraj N, Selbach M, Olsen JV, Mann M (2009) A practical guide to the MaxQuant computational platform for SILAC-based quantitative proteomics. *Nat Protoc* **4**(5)**:** 698-705

Cox J, Neuhauser N, Michalski A, Scheltema RA, Olsen JV, Mann M (2011) Andromeda: a peptide search engine integrated into the MaxQuant environment. *J Proteome Res* **10**(4)**:** 1794-1805

Grovdal LM, Stang E, Sorkin A, Madshus IH (2004) Direct interaction of Cbl with pTyr 1045 of the EGF receptor (EGFR) is required to sort the EGFR to lysosomes for degradation. *Exp Cell Res* **300**(2)**:** 388-395

Huang F, Khvorova A, Marshall W, Sorkin A (2004) Analysis of clathrin-mediated endocytosis of epidermal growth factor receptor by RNA interference. *J Biol Chem* **279**(16)**:** 16657-16661

Huang F, Kirkpatrick D, Jiang X, Gygi S, Sorkin A (2006) Differential regulation of EGF receptor internalization and degradation by multiubiquitination within the kinase domain. *Mol Cell* **21**(6)**:** 737-748

Jiang X, Sorkin A (2003) Epidermal growth factor receptor internalization through clathrin-coated pits requires Cbl RING finger and proline-rich domains but not receptor polyubiquitylation. *Traffic* **4**(8)**:** 529-543

Kall L, Storey JD, MacCoss MJ, Noble WS (2008) Assigning significance to peptides identified by tandem mass spectrometry using decoy databases. *J Proteome Res* **7**(1)**:** 29-34

Kazazic M, Bertelsen V, Pedersen KW, Vuong TT, Grandal MV, Rodland MS, Traub LM, Stang E, Madshus IH (2009) Epsin 1 is involved in recruitment of ubiquitinated EGF receptors into clathrin-coated pits. *Traffic* **10**(2)**:** 235-245

Lund KA, Opresko LK, Starbuck C, Walsh BJ, Wiley HS (1990) Quantitative analysis of the endocytic system involved in hormone-induced receptor internalization. *J Biol Chem* **265**(26)**:** 15713-15723

Madshus IH, Stang E (2009) Internalization and intracellular sorting of the EGF receptor: a model for understanding the mechanisms of receptor trafficking. *J Cell Sci* **122**(Pt 19)**:** 3433-3439

Michalski A, Cox J, Mann M (2011) More than 100,000 detectable peptide species elute in single shotgun proteomics runs but the majority is inaccessible to data-dependent LC-MS/MS. *J Proteome Res* **10**(4)**:** 1785-1793

Nagaraj N, D'Souza RC, Cox J, Olsen JV, Mann M (2010) Feasibility of large-scale phosphoproteomics with higher energy collisional dissociation fragmentation. *J Proteome Res* **9**(12)**:** 6786-6794

Olsen JV, Blagoev B, Gnad F, Macek B, Kumar C, Mortensen P, Mann M (2006) Global, in vivo, and site-specific phosphorylation dynamics in signaling networks. *Cell* **127**(3)**:** 635-648

Olsen JV, de Godoy LM, Li G, Macek B, Mortensen P, Pesch R, Makarov A, Lange O, Horning S, Mann M (2005) Parts per million mass accuracy on an Orbitrap mass spectrometer via lock mass injection into a C-trap. *Mol Cell Proteomics* **4**(12)**:** 2010-2021

Opresko LK, Wiley HS (1987) Receptor-mediated endocytosis in Xenopus oocytes. II. Evidence for two novel mechanisms of hormonal regulation. *J Biol Chem* **262**(9)**:** 4116-4123

Penengo L, Mapelli M, Murachelli AG, Confalonieri S, Magri L, Musacchio A, Di Fiore PP, Polo S, Schneider TR (2006) Crystal structure of the ubiquitin binding domains of rabex-5 reveals two modes of interaction with ubiquitin. *Cell* **124**(6)**:** 1183-1195

Schroeder MJ, Shabanowitz J, Schwartz JC, Hunt DF, Coon JJ (2004) A neutral loss activation method for improved phosphopeptide sequence analysis by quadrupole ion trap mass spectrometry. *Anal Chem* **76**(13)**:** 3590-3598

Sigismund S, Argenzio E, Tosoni D, Cavallaro E, Polo S, Di Fiore PP (2008) Clathrin-mediated internalization is essential for sustained EGFR signaling but dispensable for degradation. *Dev Cell* **15**(2)**:** 209-219

Sigismund S, Woelk T, Puri C, Maspero E, Tacchetti C, Transidico P, Di Fiore PP, Polo S (2005) Clathrin-independent endocytosis of ubiquitinated cargos. *Proc Natl Acad Sci U S A* **102**(8)**:** 2760-2765

Wiley HS, Cunningham DD (1982) The endocytotic rate constant. A cellular parameter for quantitating receptor-mediated endocytosis. *J Biol Chem* **257**(8)**:** 4222-4229

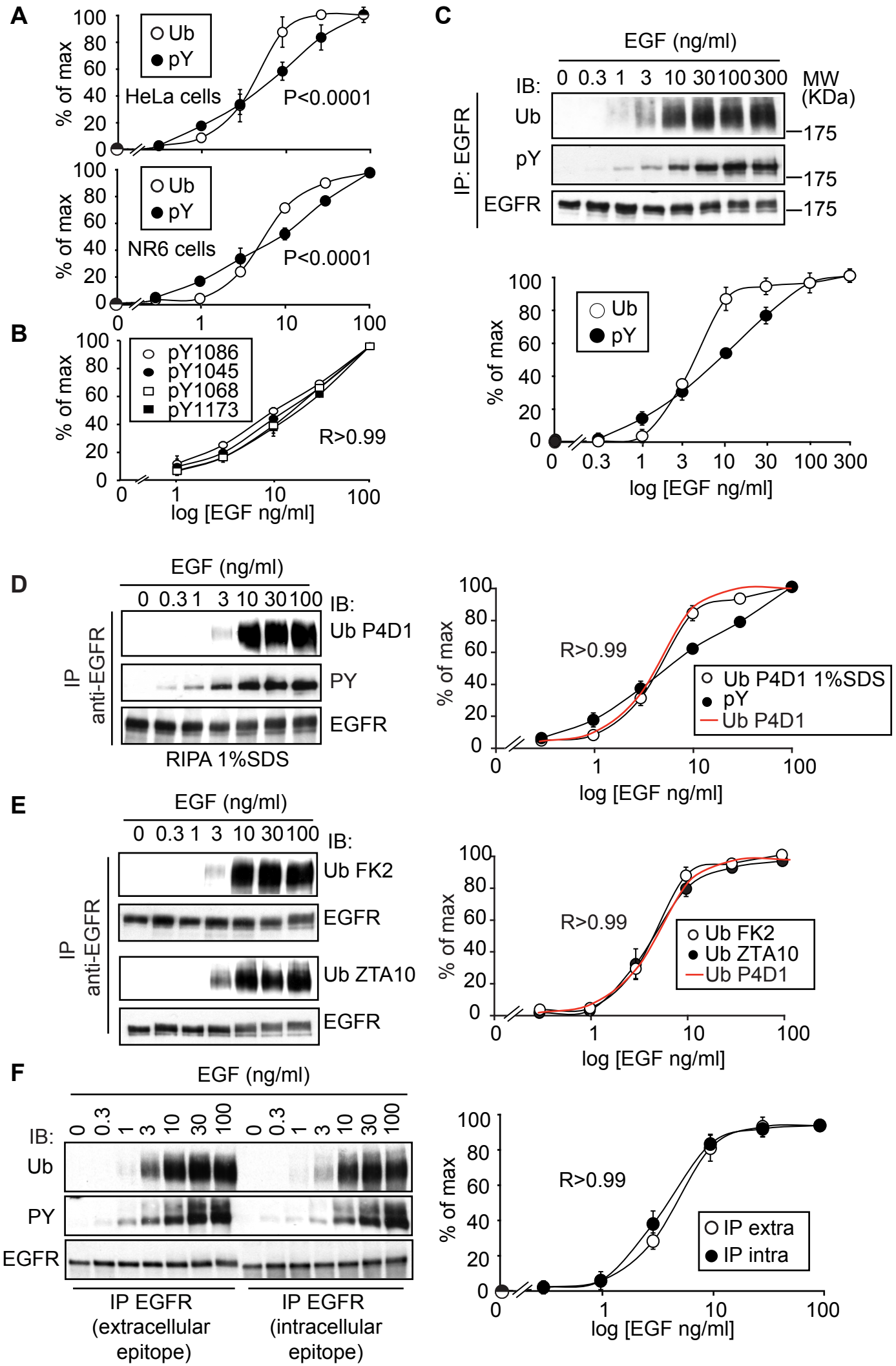

Supplementary Figure 1

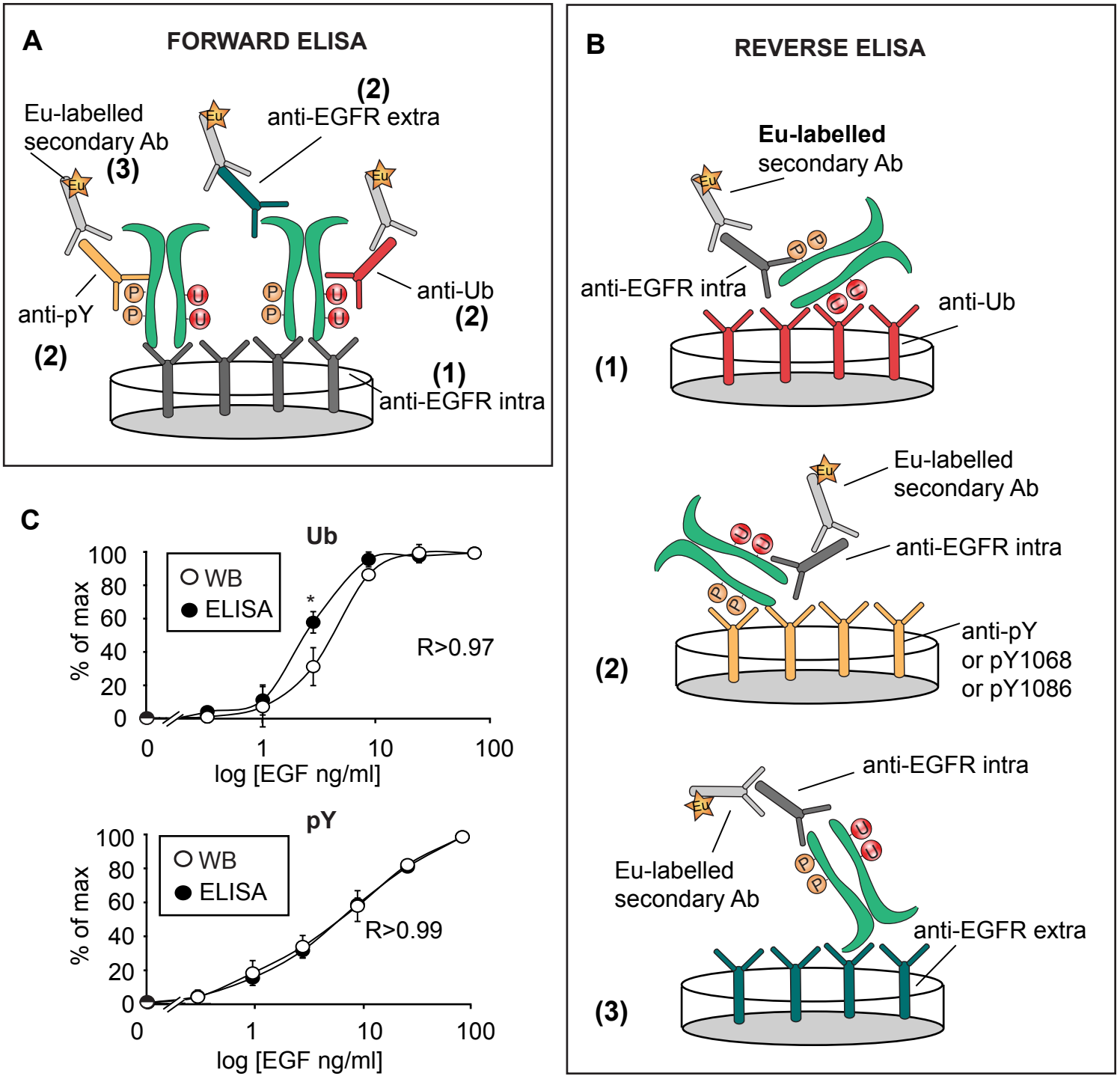

Supplementary Figure 2

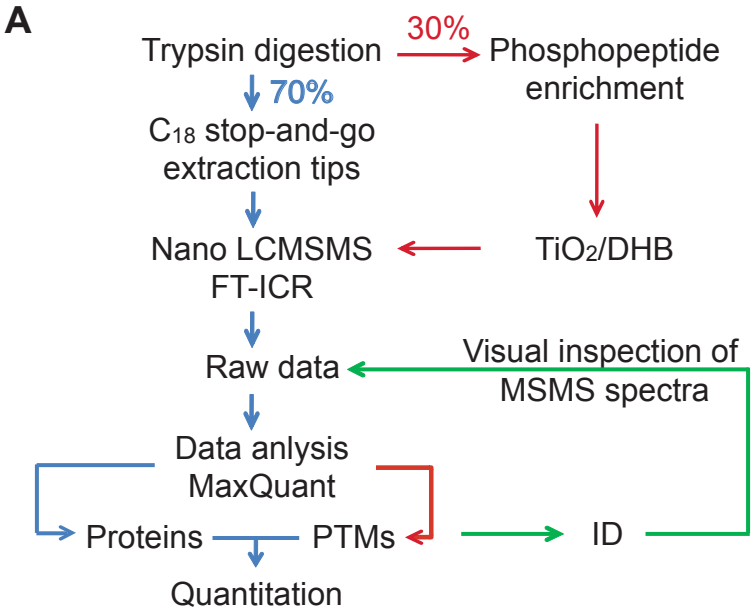

Supplementary Figure 3A

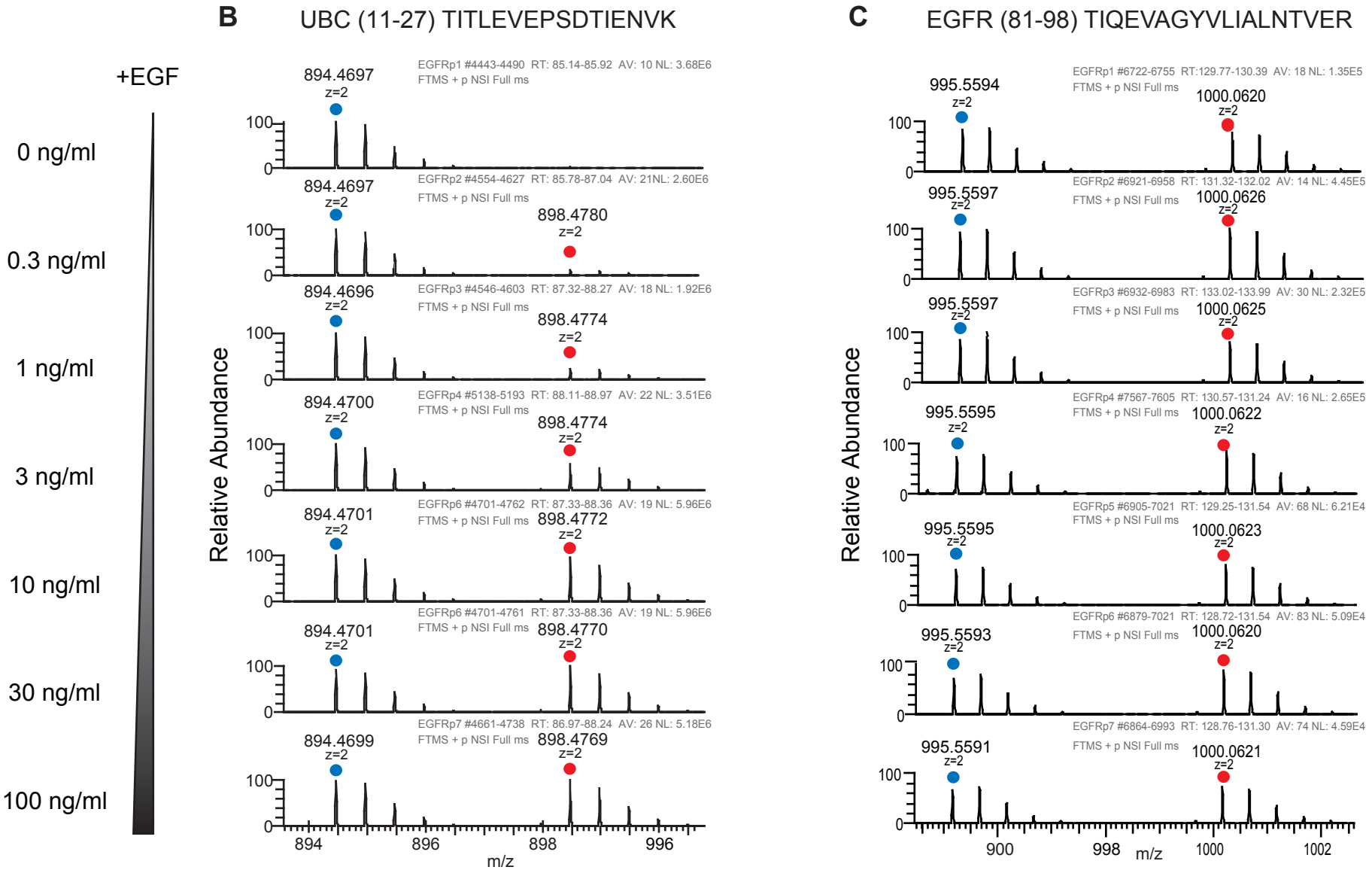

Supplementary Figure 3B-C

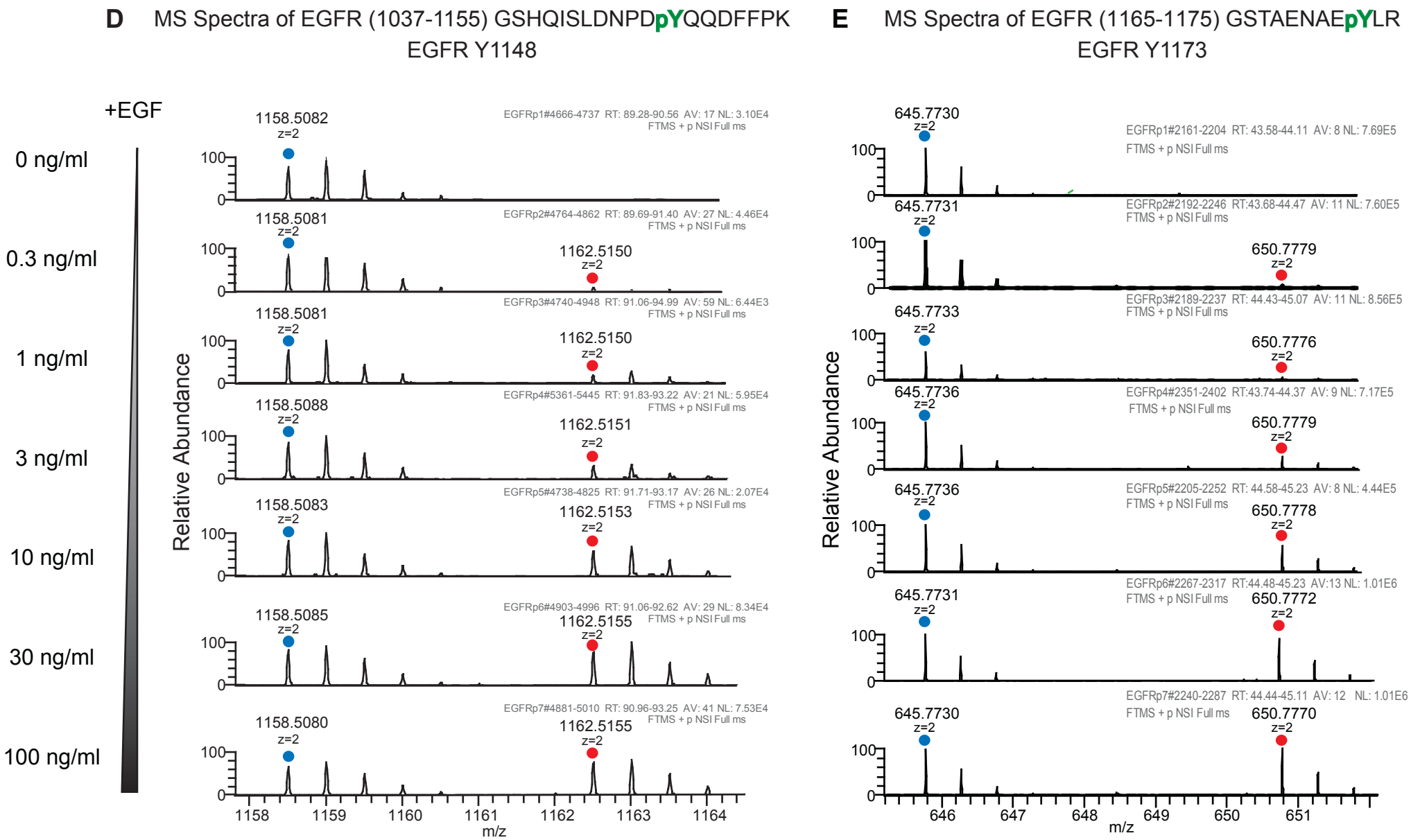

SupplementaryFigure 3D-E

F MS Spectra of EGFR (1076-1097) RPAGSVQNPV**pY**HNQPLNPAPSR

EGFR Y1086

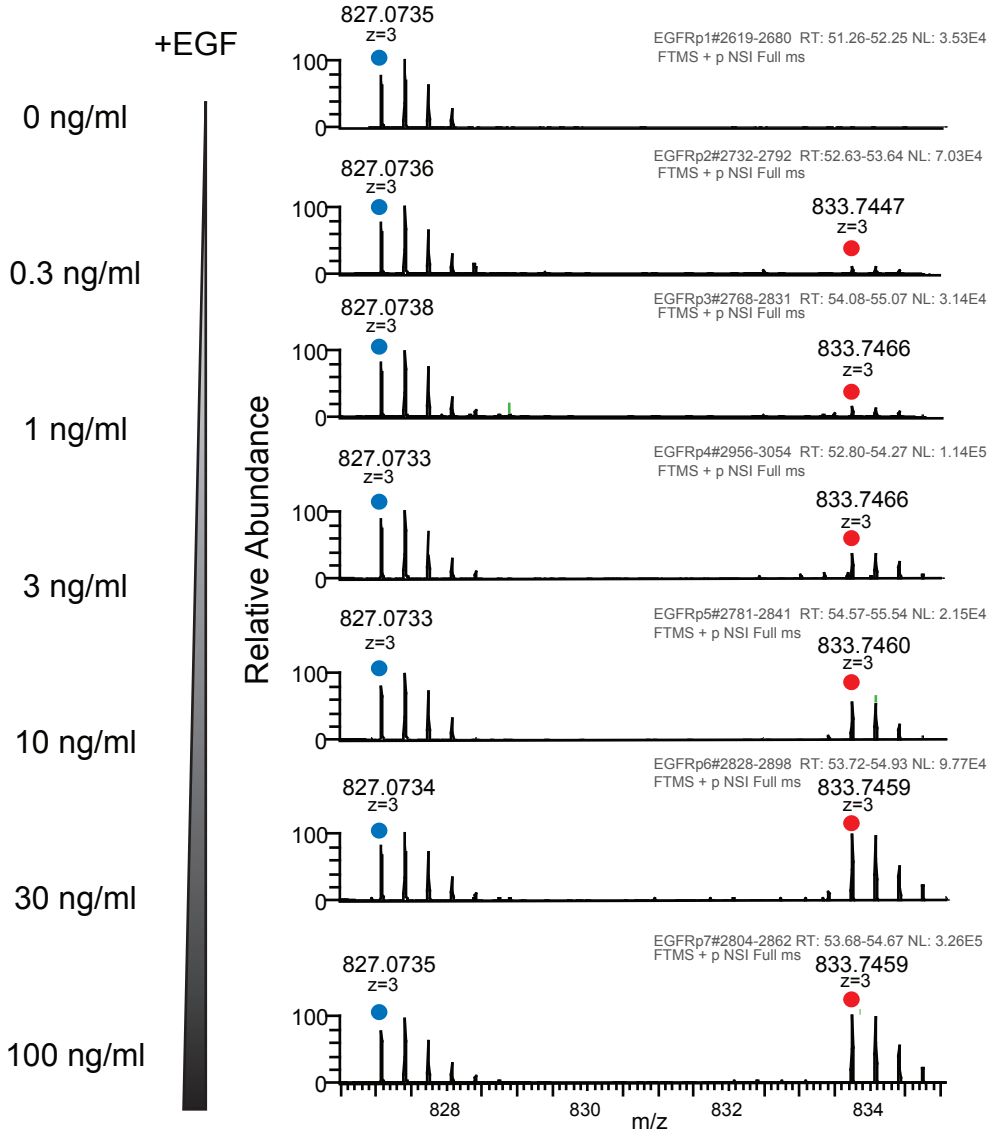

G MS Spectra of EGFR (691-704) I**K(glygly)**VLGSGAFGTVYK

EGFR K692

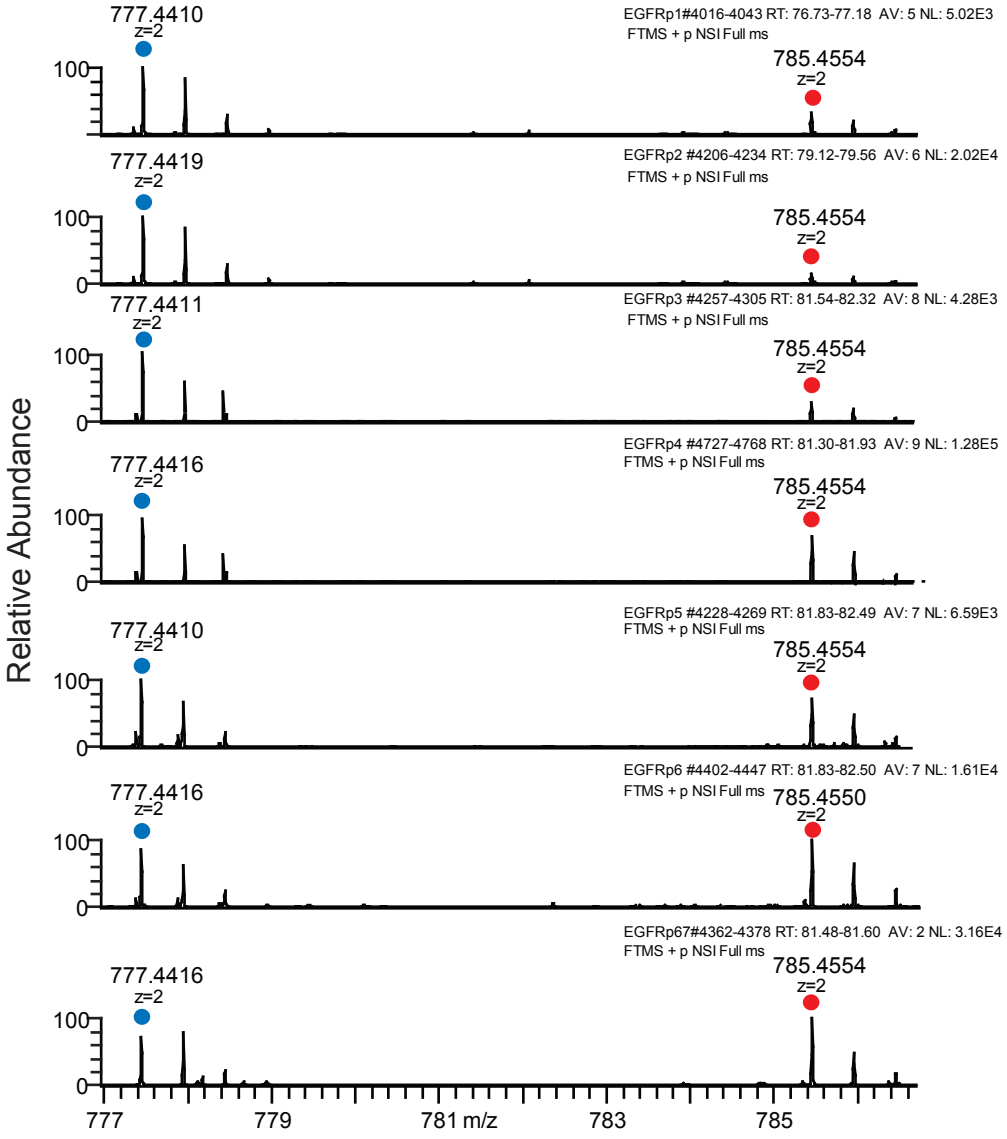

Supplementary Figure 3F-G

H Tandem MS Spectrum and Full Annotation of EGFR Y(1148)

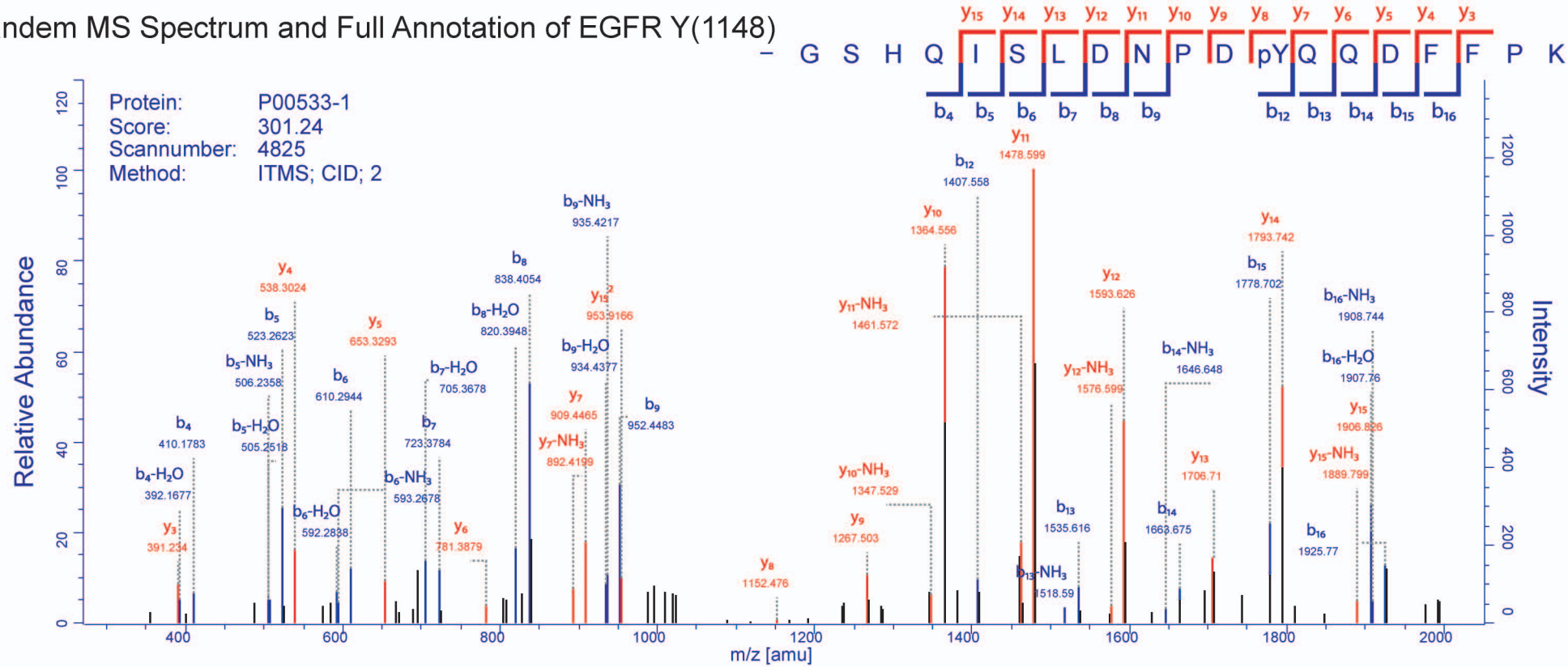

b ion					y ion		y + ion	
Δ dalton	mass		seq		mass	Δ dalton	mass	Δ dalton
	58.0287	1	G	19				
	145.061	2	S	18	2258.98		2258.98	
	282.12	3	H	17	2171.94		2171.94	
0.09481	410.178	4	Q	16	2034.88		2034.88	
0.04847	523.262	5	I	15	1906.83	0.05021	953.917	0.4648
0.09078	610.294	6	S	14	1793.74	0.16077	1793.74	
0.10468	723.378	7	L	13	1706.71	0.25423	1706.71	
0.12545	838.405	8	D	12	1593.63	0.17187	1593.63	
0.04338	952.448	9	N	11	1478.6	0.06778	1478.6	
	1049.5	10	P	10	1364.56	0.12483	1364.56	
	1164.53	11	D	9	1267.5	0.00065	1267.5	
0.14456	1407.56	12	Y	8	1152.48	0.01359	1152.48	
0.10988	1535.62	13	Q	7	909.446	0.16622	909.446	
0.30676	1663.67	14	Q	6	781.388	0.07236	781.388	
0.26376	1778.7	15	D	5	653.329	0.00135	653.329	
0.23525	1925.77	16	F	4	538.302	0.09592	538.302	
	2072.84	17	F	3	391.234	0.16299	391.234	
	2169.89	18	P	2	244.166		244.166	
		19	K	1	147.113		147.113	

precursor information

Mass:	2315.00046
m/z:	1158.50751
Charge:	2+
Retention time:	90.75327
Score:	301.2354
Mass Error [ppm]:	0.6958
PEP:	2.52E-30
Precursor Type:	MULTI

general information

Annotation:	14 of 19
Amino acid Coverage:	74 %
Intensity Coverage:	63 %

Supplementary Figure 3H

I Tandem MS Spectrum and Full Annotation of EGFR Y(1173)

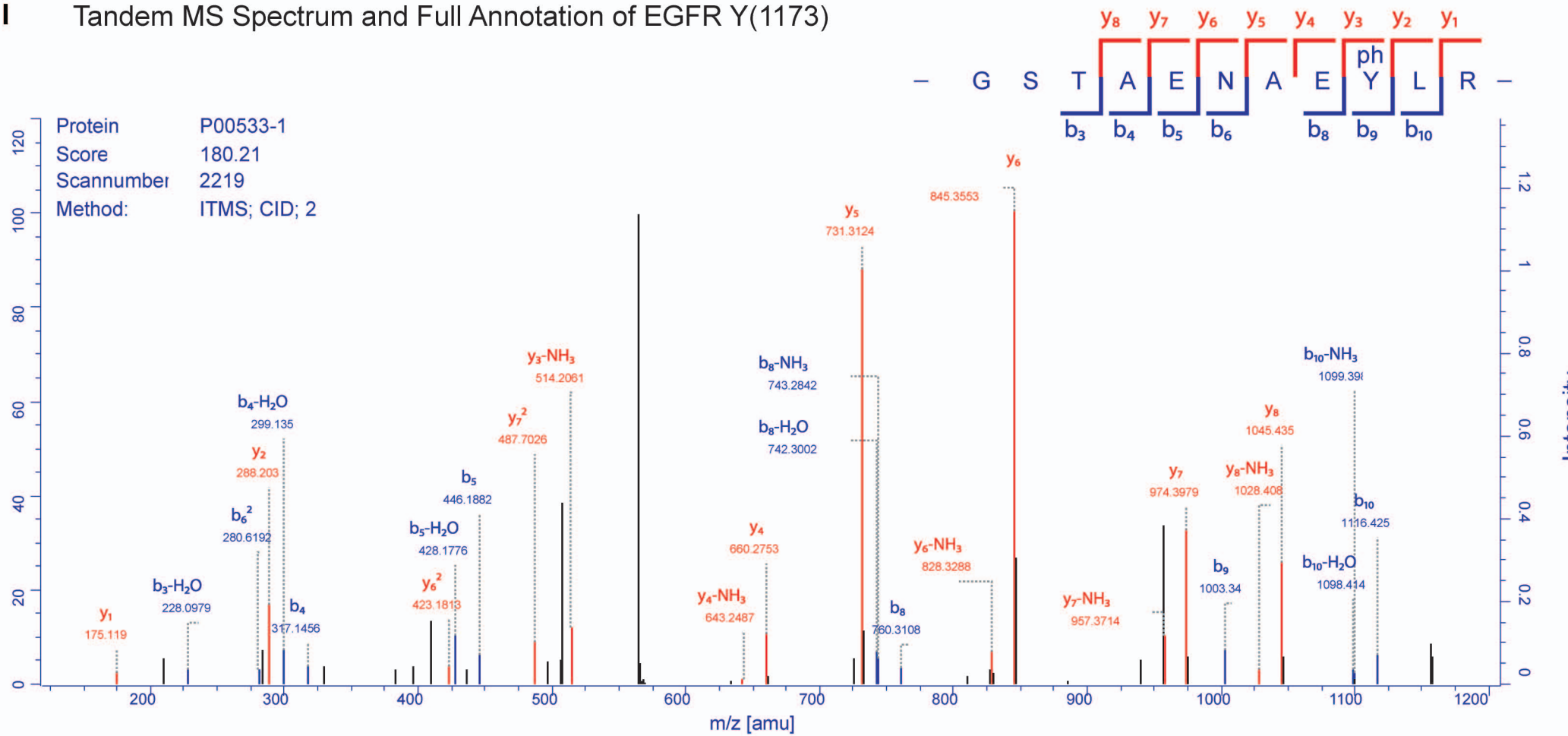

b + ion		b ion					y ion		y 2 ion	
Δ dalton	mass	Δ dalton	mass		seq		mass	Δ dalton	mass	Δ dalton
	58.03		58.03	1	G	11				
	145.1		145.1	2	S	10	1234		1234	
	246.1		246.1	3	T	9	1146		1146	
	317.1	0.078	317.1	4	A	8	1045	0.04	1045	
	446.2	0.034	446.2	5	E	7	974.4	0.041	487.7	0.114
0.506	280.6		560.2	6	N	6	845.4	0.017	423.2	0.226
	631.3		631.3	7	A	5	731.3	0.061	731.3	
	760.3	0.016	760.3	8	E	4	660.3	0.077	660.3	
	1003	0.067	1003	9	Y	3	531.2		531.2	
	1116	0.101	1116	10	L	2	288.2	0.094	288.2	
				11	R	1	175.1	0.035	175.1	

precursor information

Mass:	1289.52931
m/z:	645.77193
Charge:	2+
Retention time:	44.74818
Score:	180.2093
Mass Error [ppm]:	0.30598
PEP:	2.1777E-05
Precursor Type:	MULTI

general information

Annotation:	9 of 11
Amino acid Coverage:	82 %
Intensity Coverage:	55 %

Supplementary Figure 3I

J Tandem MS Spectrum and Full Annotation of EGFR Y(1086)

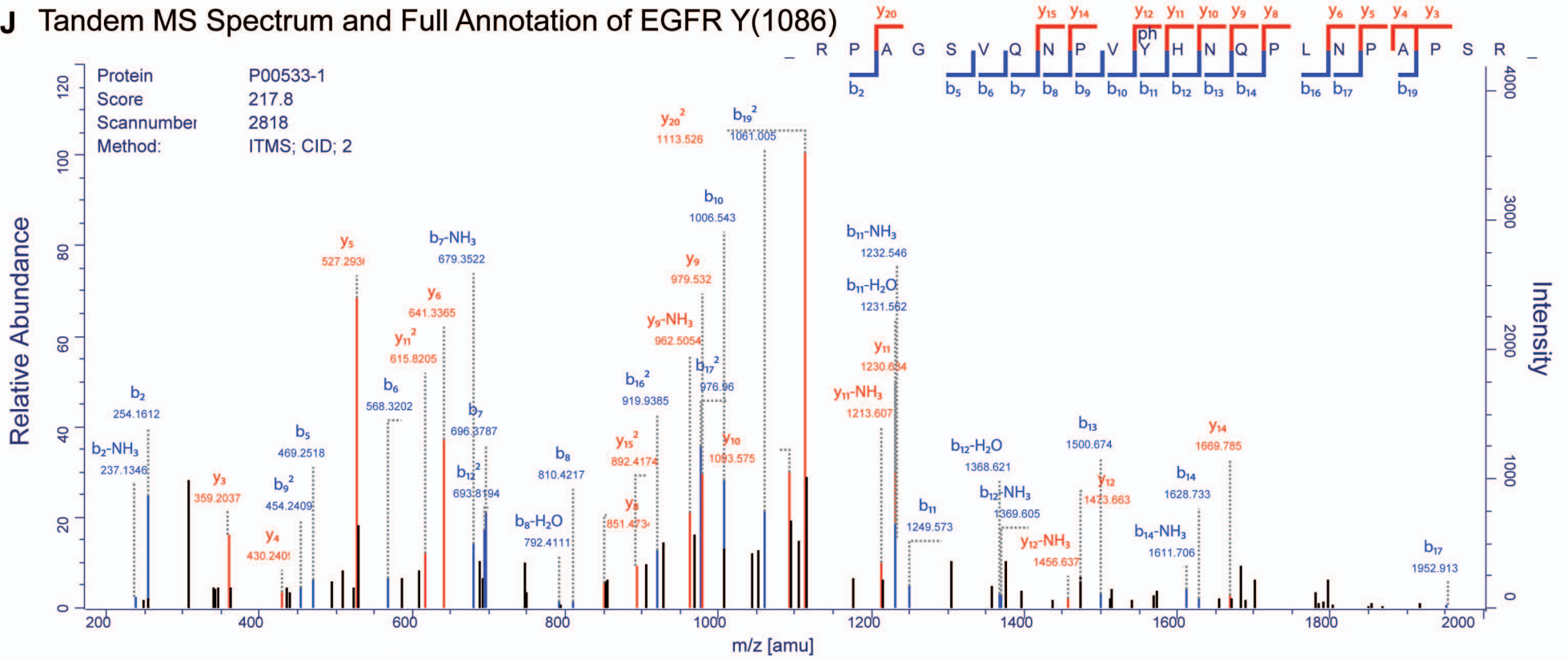

b +ion Δ dalton	b +ion mass	b ion Δ dalton	b ion mass		seq		y ion mass	y ion Δ dalton	y + ion mass	y + ion Δ dalton
	157.1		157.1	1	R	22				
	254.2	0.016	254.2	2	P	21	2323		2323	
	325.2		325.2	3	A	20	2226		1114	0.336
	382.2		382.2	4	G	19	2155		2155	
	469.3	0.241	469.3	5	S	18	2098		2098	
	568.3	0.16	568.3	6	V	17	2011		2011	
	696.4	0.118	696.4	7	Q	16	1912		1912	
	810.4	0.28	810.4	8	N	15	1784		892.4	0.299
0.303	454.2		907.5	9	P	14	1670	0.072	1670	
	1007	0.061	1007	10	V	13	1573		1573	
	1250	0.025	1250	11	Y	12	1474	0.344	1474	
0.225	693.8		1387	12	H	11	1231	0.071	615.8	0.329
	1501	0.033	1501	13	N	10	1094	0.075	1094	
	1629	0.239	1629	14	Q	9	979.5	0.073	979.5	
	1726		1726	15	P	8	851.5	0.001	851.5	
0.246	919.9		1839	16	L	7	754.4		754.4	
0.355	977	0.172	1953	17	N	6	641.3	0.02	641.3	
	2050		2050	18	P	5	527.3	0.05	527.3	
0.068	1061		2121	19	A	4	430.2	0.072	430.2	
	2218		2218	20	P	3	359.2	0.134	359.2	
	2305		2305	21	S	2	262.2		262.2	
				22	R	1	175.1		175.1	

precursor information

Mass:	2478.19579
m/z:	827.07254
Charge:	3+
Retention time:	53.88966
Score:	217.8019
Mass Error [ppm]:	1.6286
PEP:	1.2863E-10
Precursor Type:	MULTI

general information

Annotation:	18 of 22
Amino acids Coverage:	82 %
Intensity Coverage:	60 %

Supplementary Figure 3J

K Tandem MS Spectrum and Full Annotation of EGFR Ub-K(692)

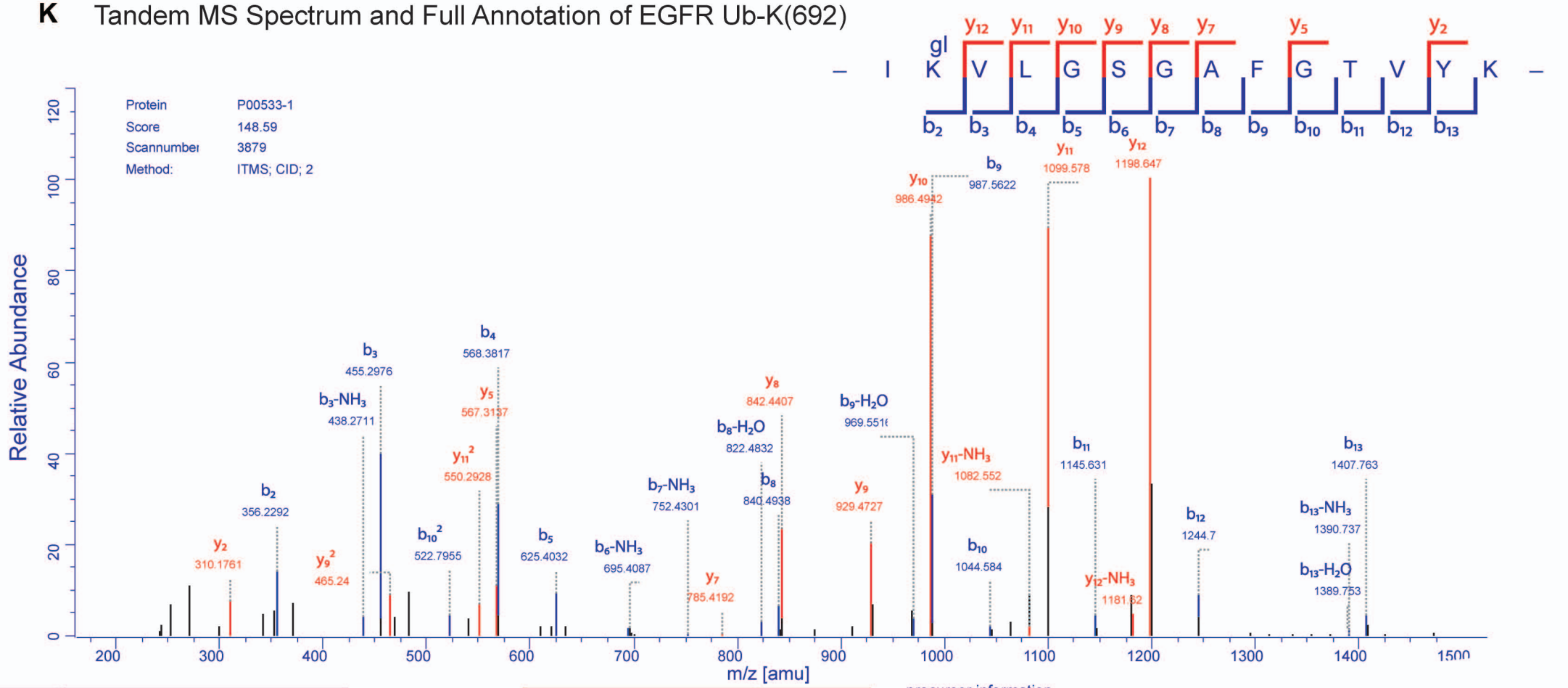

b^2 ion		b ion					y ion		y^2 ion	
Δ dalton	mass	Δ dalton	mass		seq		mass	Δ dalton	mass	Δ dalton
	114.1		114.1	1	I	14				
	356.2	0.018	356.2	2	K	13	1441		1441	
	455.3	0.059	455.3	3	V	12	1199	0.05	1199	
	568.4	0.032	568.4	4	L	11	1100	0.066	550.3	0.069
	625.4	0.074	625.4	5	G	10	986.5	0.004	986.5	
	712.4		712.4	6	S	9	929.5	0.071	465.2	0.178
	769.5		769.5	7	G	8	842.4	0.02	842.4	
	840.5	0.039	840.5	8	A	7	785.4	0.292	785.4	
	987.6	0.047	987.6	9	F	6	714.4		714.4	
0.471	522.8	0.143	1045	10	G	5	567.3	0.081	567.3	
	1146	0.044	1146	11	T	4	510.3		510.3	
	1245	0.047	1245	12	V	3	409.2		409.2	
	1408	0.177	1408	13	Y	2	310.2	0.091	310.2	
				14	K	1	147.1		147.1	

precursor information

Mass	1552.86503
m/z:	777.43979
Charge:	2+
Retention time:	78.89876
Score:	148.5885
Mass Error [ppm]:	2.3816
PEP	0.001338

general information

Annotation:	12 of 14
Amino acid Coverage:	86 %
Intensity Coverage:	73 %

Supplementary Figure 3K

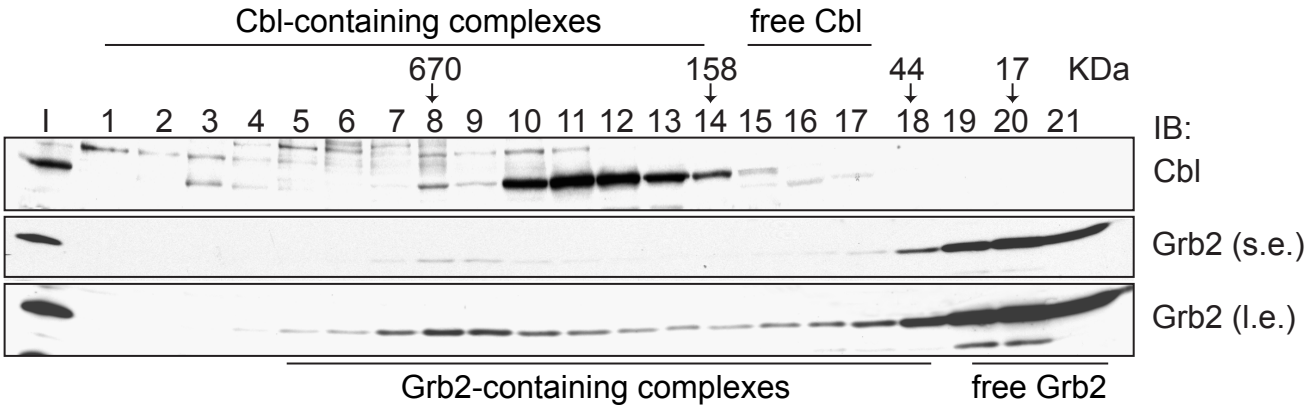

Supplementary Figure 4

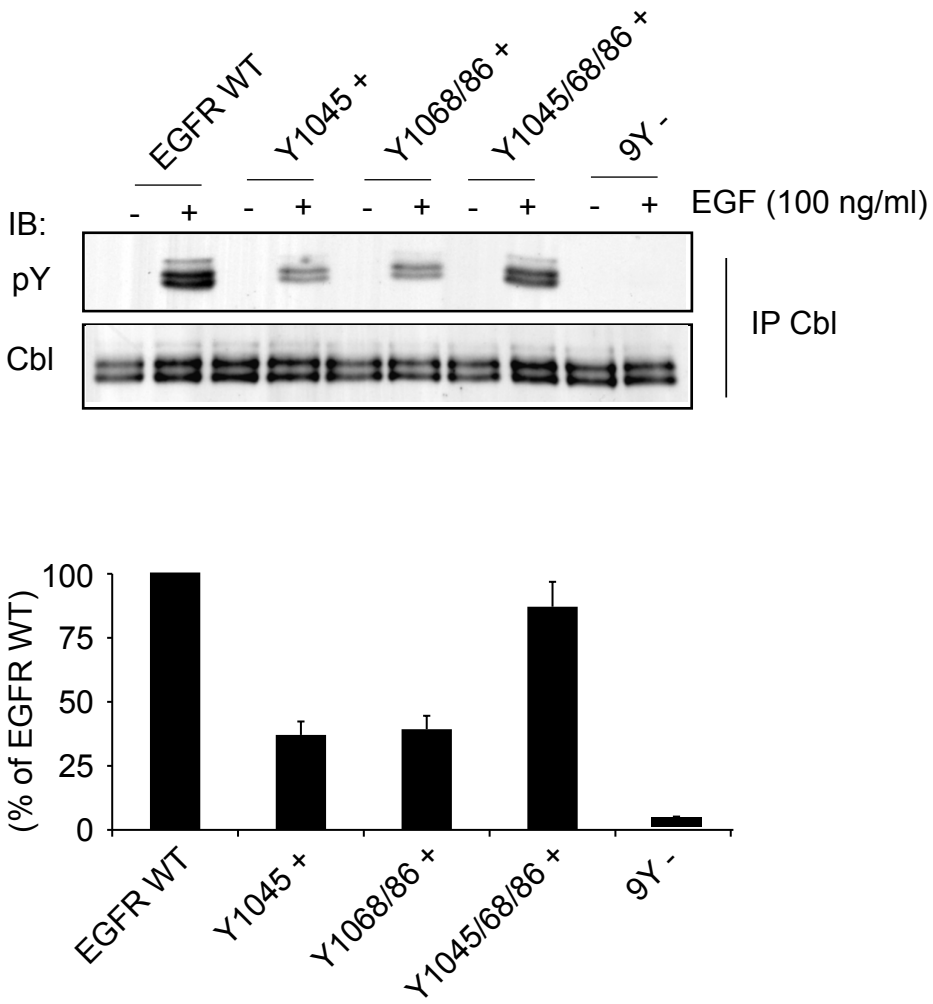

Supplementary Figure 5

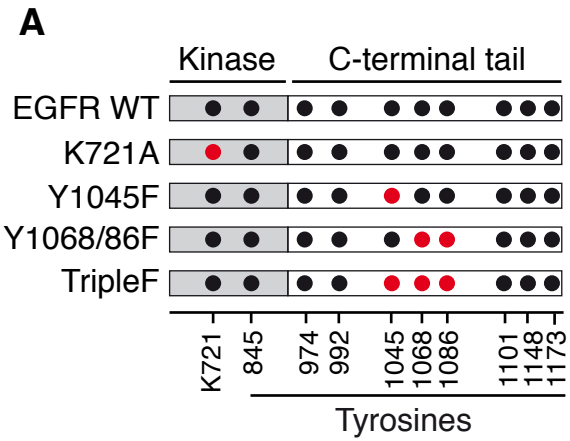

B

	Surface EGFRs (rec/cell x10³)
EGFR WT	250
K721A	210
Y1045F	260
Y1068/86F	250
Y1045/68/86F	240

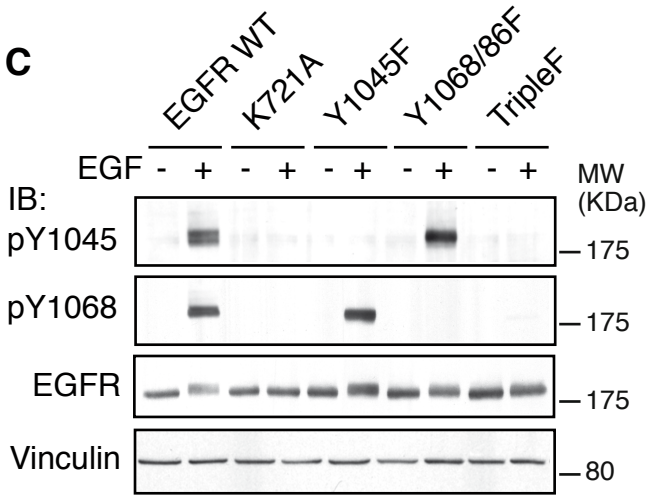

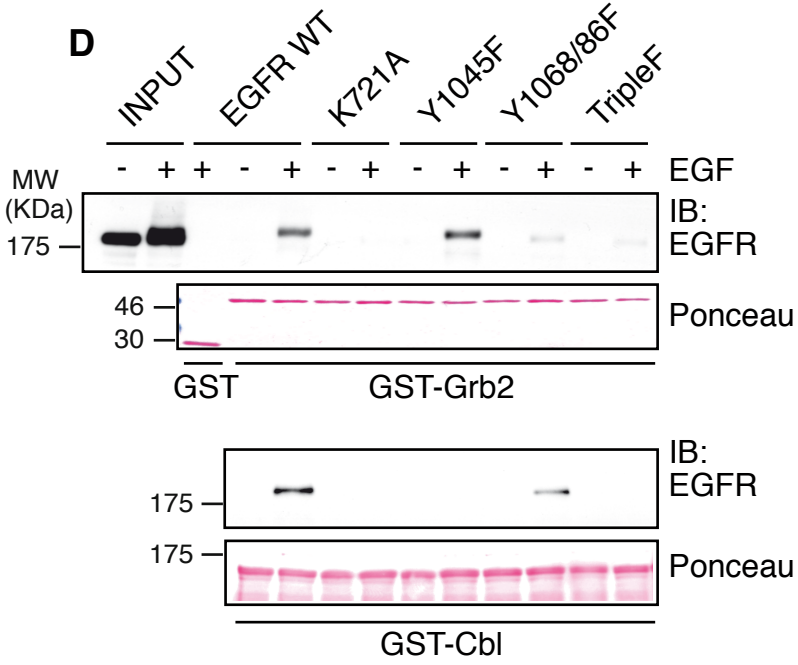

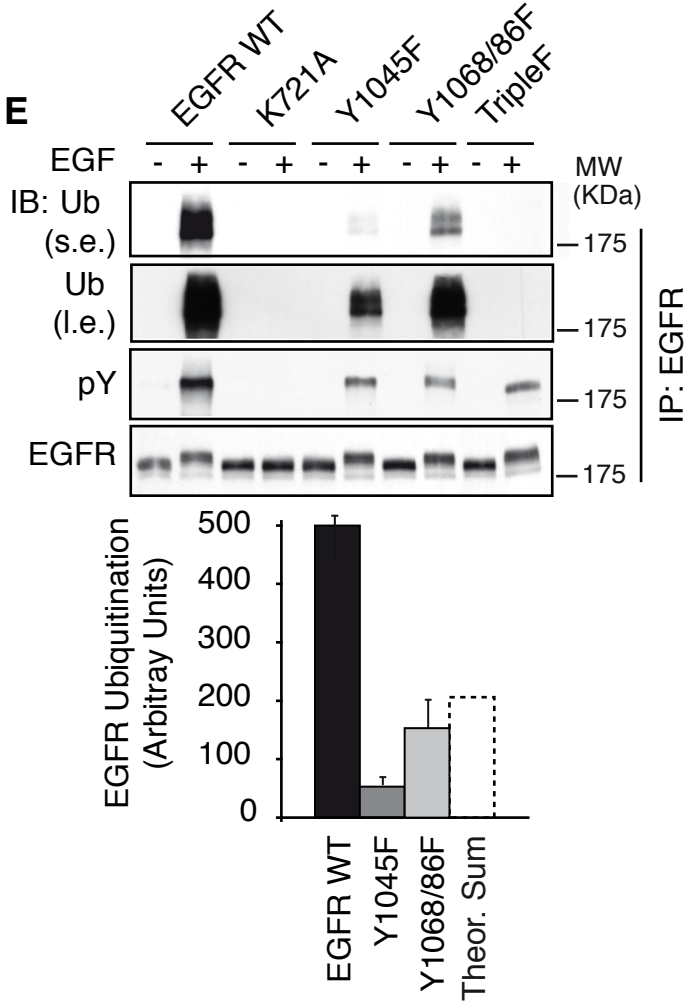

F

	EGFR WT (Ke)	TripleF (Ke)
	Low EGF (1 ng/ml)	
Control	0.084	0.051
Clath KD	0.005	0.005
Filipin	0.084	0.052
	High EGF (30 ng/ml)	
Control	0.071	0.043
Clath KD	0.027	0.004
Filipin	0.048	0.041

Supplementary Figure 6

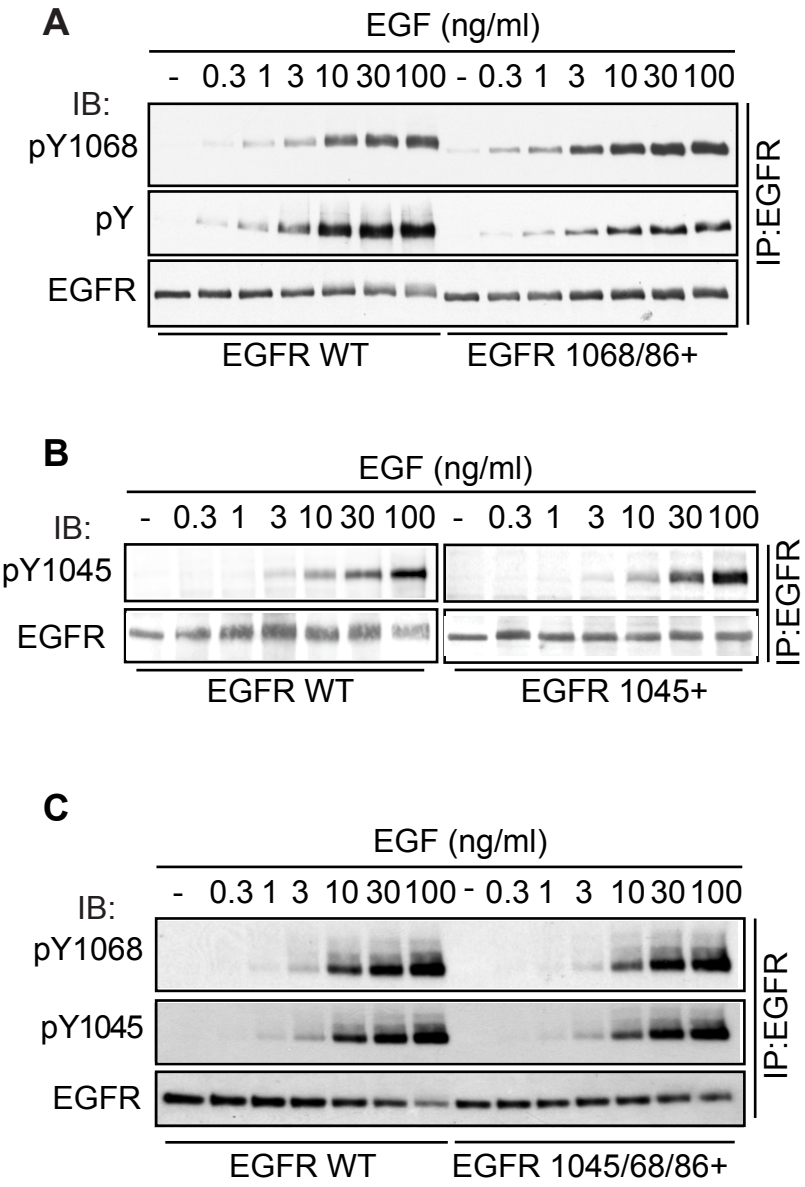

Supplementary Figure 7

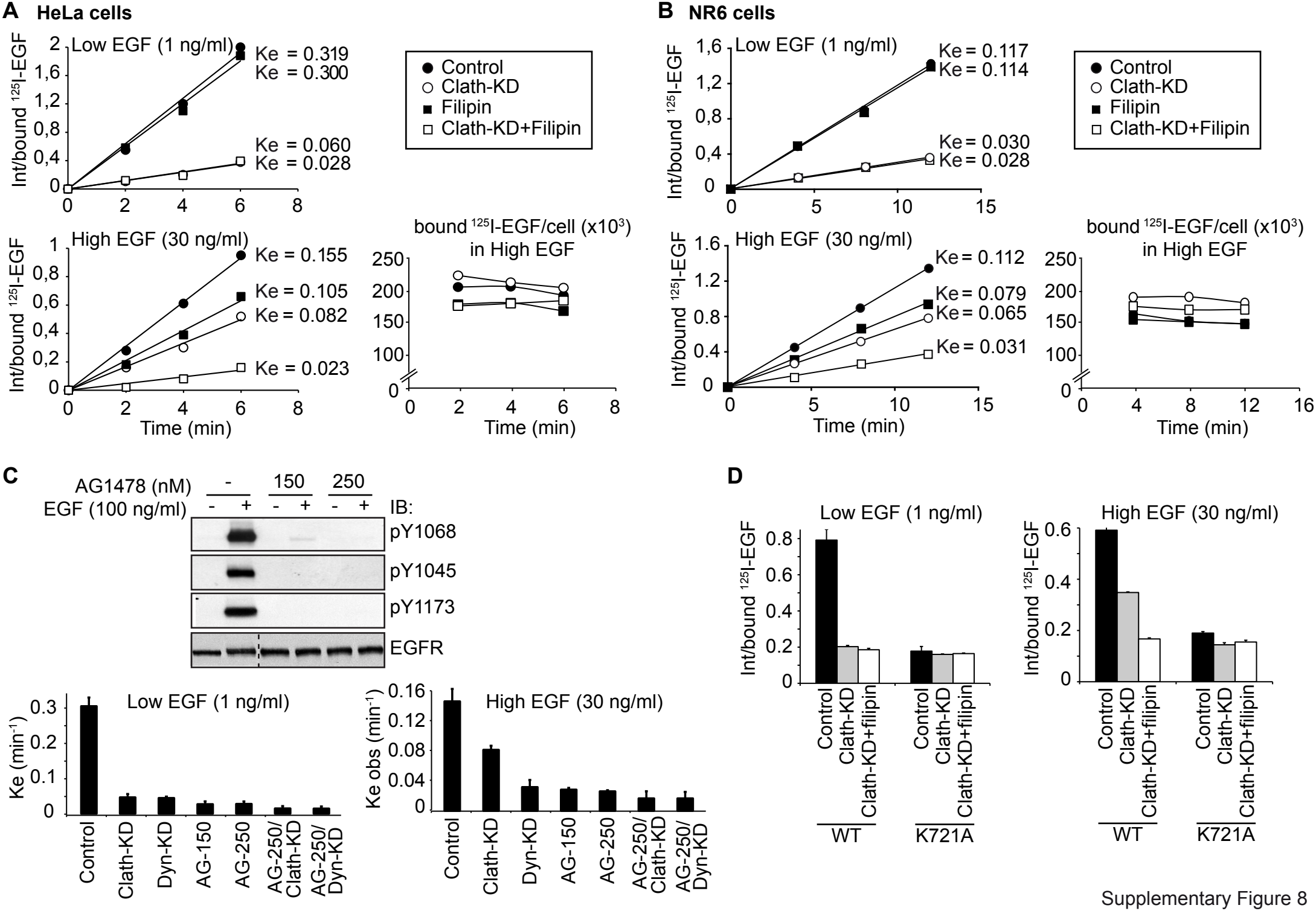

Supplementary Figure 8

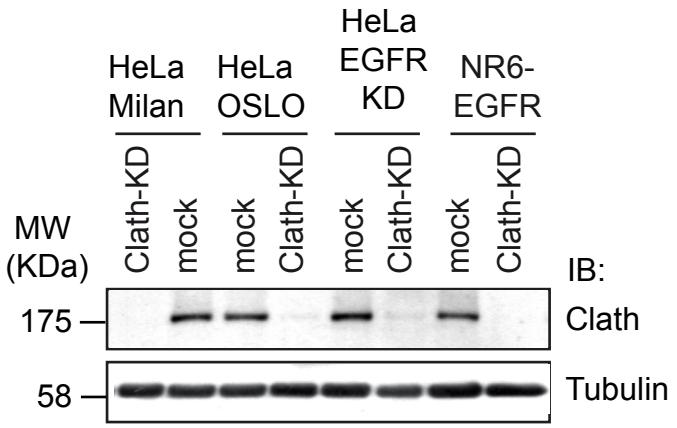

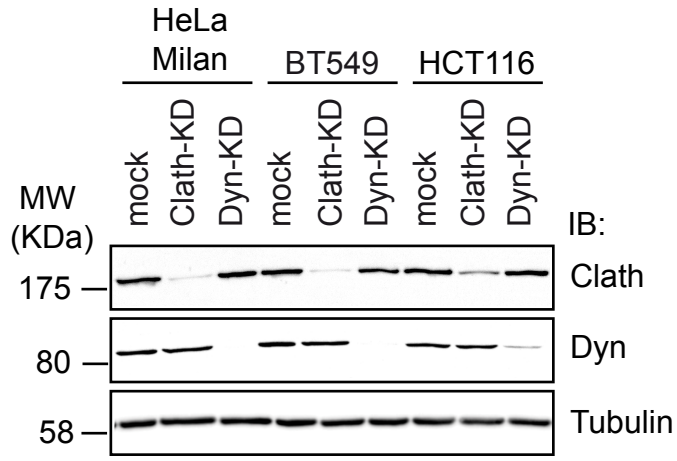

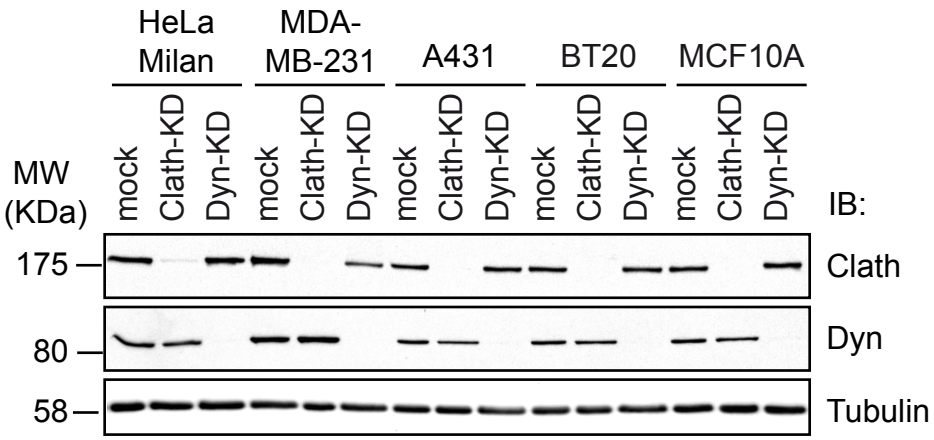

Supplementary Figure 9

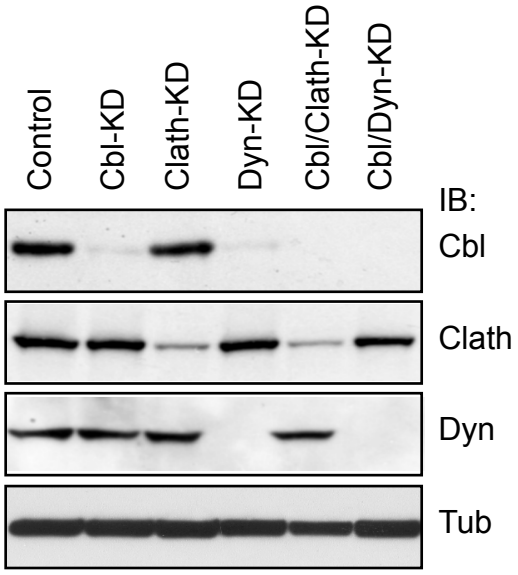

Supplementary Figure 10

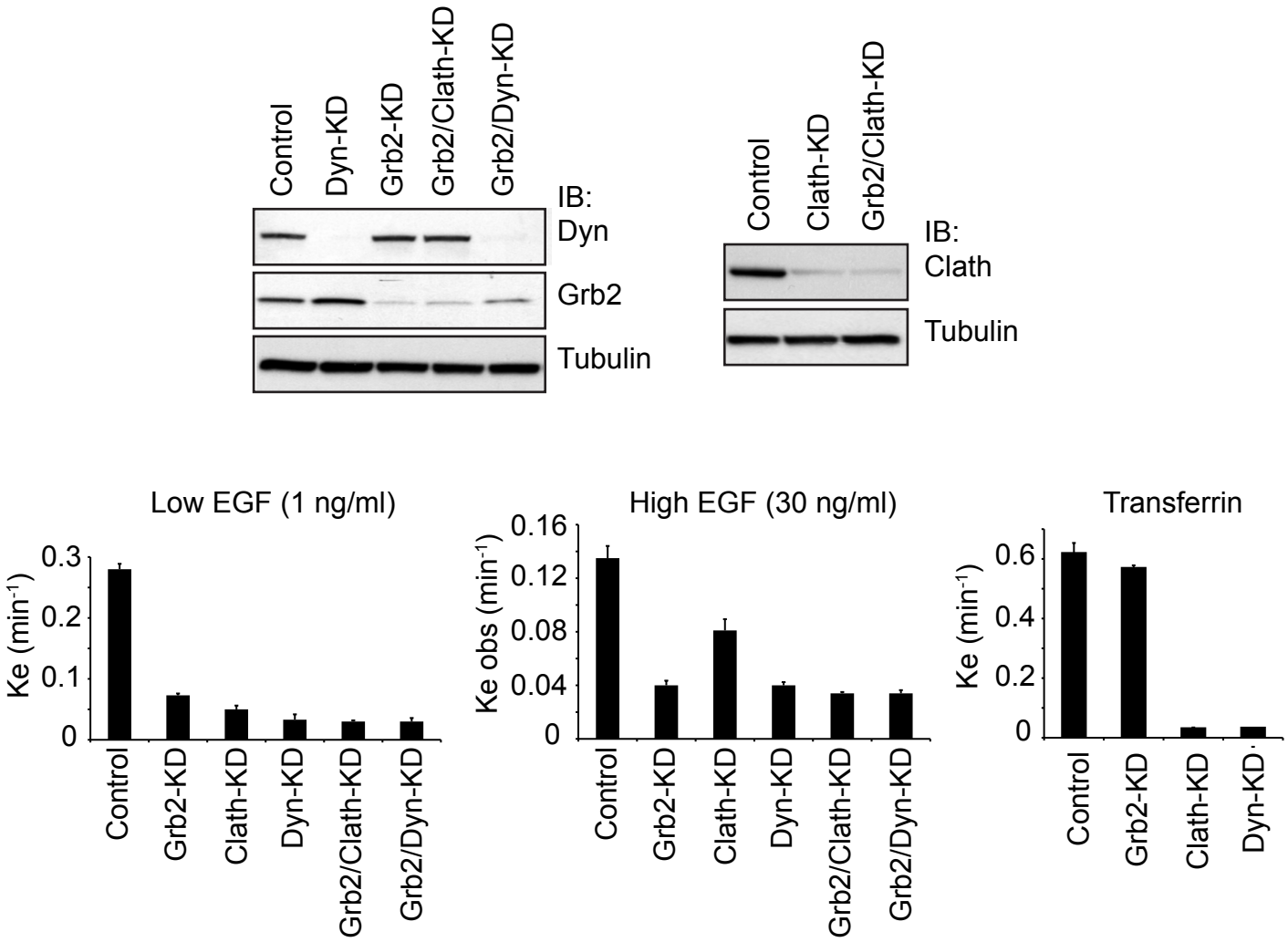

Supplementary Figure 11

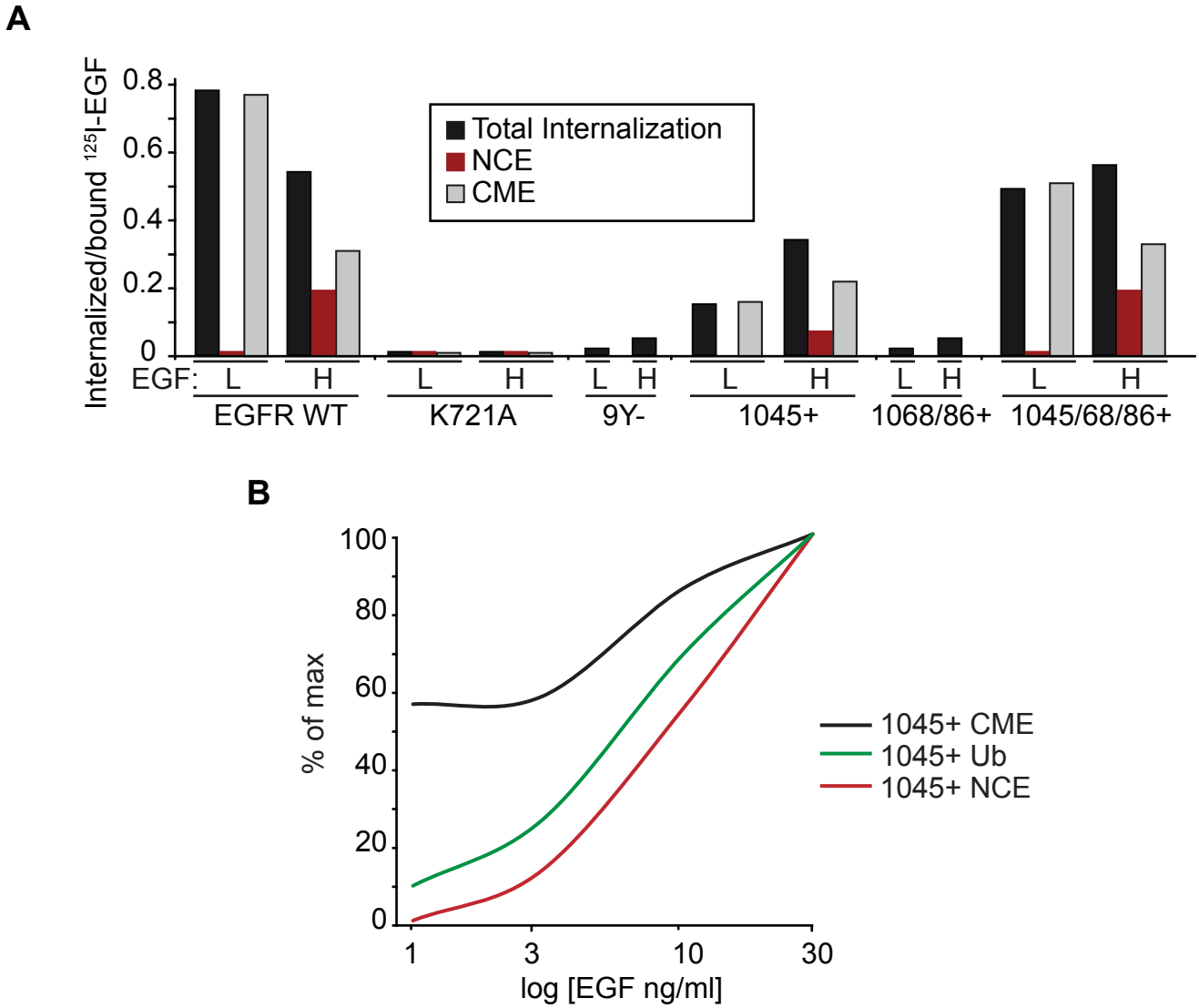

Supplementary Figure 12